Journal of Medicinal Chemistry

pubs.acs.org/jmc Article

Design, Synthesis, and Evaluation of VHL-Based EZH2 Degraders to Enhance Therapeutic Activity against Lymphoma

Yalin Tu,[§] Yameng Sun,[§] Shuang Qiao,[§] Yao Luo, Panpan Liu, Zhong-Xing Jiang, Yumin Hu, Zifeng Wang, Peng Huang,* and Shijun Wen*

Cite This: *J. Med. Chem.* 2021, 64, 10167−10184 Read Online

ACCESS | Metrics & More | Article Recommendations | Supporting Information

ABSTRACT: Traditional EZH2 inhibitors are developed to suppress the enzymatic methylation activity, and they may have therapeutic limitations due to the nonenzymatic functions of EZH2 in cancer development. Here, we report proteolysis-target chimera (PROTAC)-based EZH2 degraders to target the whole EZH2 in lymphoma. Two series of EZH2 degraders were designed and synthesized to hijack E3 ligase systems containing either von Hippel−Lindau (VHL) or cereblon (CRBN), and some VHL-based compounds were able to mediate EZH2 degradation. Two best degraders, YM181 and YM281, induced robust cell viability inhibition in diffuse large B-cell lymphoma (DLBCL) and other subtypes of lymphomas, outperforming a clinically used EZH2 inhibitor EPZ6438 (tazemetostat) that was only effective against DLBCL. The EZH2 degraders displayed promising antitumor activities in lymphoma xenografts and patient-derived primary lymphoma cells. Our study demonstrates that EZH2 degraders have better therapeutic activity than EZH2 inhibitors, which may provide a potential anticancer strategy to treat lymphoma.

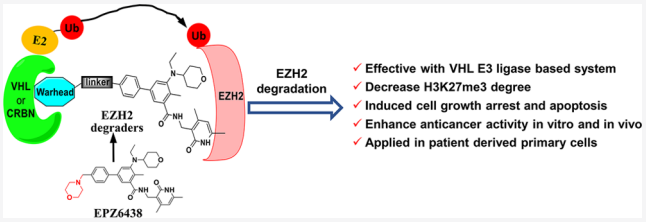

INTRODUCTION

EZH2 is the enzymatic subunit of polycomb repressive complex 2 (PRC2) that mainly trimethylate lysine 27 of histone H3 (H3K27) to silence the gene transcription.[1−3] Either overexpression or gain-of-function mutation of EZH2 is observed in various tumors, including lymphoma, especially diffuse large B-cell lymphoma (DLBCL), T-cell acute lymphoblastic leukemia, breast cancer, and prostate cancer.[4−6] The oncogenic roles of EZH2 are often attributed to its end-product H3K27me3-mediated epigenetic silencing of tumor suppressor genes.[7] The loss of mutation of specific subunits of other chromatin remodeling complexes that antagonize PRC2 activity, like the SWI/SNF complex, is another major reason for the activation of EZH2.[6] For example, the loss of the SWI/SNF subunit INI1 (encoded by *SMARCB1*) leads to constitutive EZH2 activation in nearly all epithelioid sarcomas.[8,9] A broad role for EZH2 in the progression of cancers with mutations of the SWI/SNF subunits ARID1A, PBRM1, and SMARCA4 has also been demonstrated in both cell lines and in vivo models.[10,11]

Many compounds that inhibit the methylation enzymatic activity of EZH2 are developed and show promising antitumor efficacy in preclinical and clinical trials in hematologic malignancies as well as solid tumors that exhibit strong EZH2 dependencies due to synthetic lethality with the aforementioned SWI/SNF subunit mutations.[6,12] In 2020, the most advanced EZH2 inhibitor EPZ6438 (tazemetostat) has been approved by FDA for the treatment of metastatic and locally advanced epithelioid sarcoma.[13] These inhibitors often bind to the SET domain of EZH2 and compete with the cofactor *S*-adenosylmethionine (SAM) without affecting the protein stability of EZH2.[14,15] However, increasing evidence has revealed that the oncogenic function of EZH2 is not entirely dependent on its enzymatic activity. The whole EZH2 protein itself is also correlated with tumor proliferation, independent of its H3K27 trimethylation activity.[5,10,16,17] Meanwhile, some drawbacks of current EZH2 inhibitors are uncovered, for example, excessive dosage, acquired resistance, and drug insensitivity to most solid tumors.[18,19] Therefore, we hypothesized that the therapeutic gains from abrogating the whole EZH2 protein rather than simply inhibiting its enzymatic activity might be better in EZH2-dependent cancers, and the development of EZH2-targeting degraders is demanded.

Cells can maintain proteins in a well-preserved homeostasis using the natural ubiquitin−proteasome degradation system in which ubiquitination is the initial key process. When ubiquitin, a small protein, tags the targeted proteins that are accumulated abnormally, the ubiquitylated proteins will be subjected to the

Received: March 13, 2021
Published: July 1, 2021

https://doi.org/10.1021/acs.jmedchem.1c00460
J. Med. Chem. 2021, 64, 10167−10184

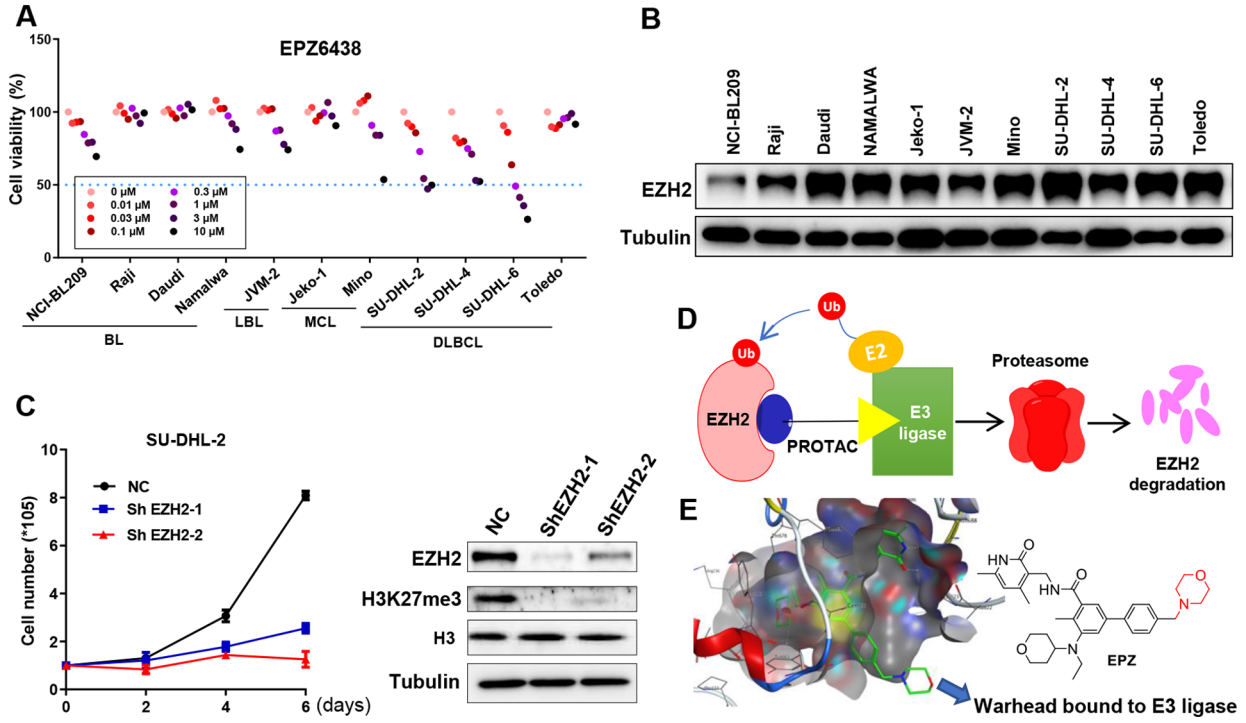

Figure 1. Strategy to develop EZH2 degraders based on PROTAC technology. (A) MTS cell viability analysis in different lymphoma cell lines treated with indicated concentrations of EPZ6438 for 5 days. (B) Western blot analysis of EZH2 protein levels in different lymphoma cell lines. Tubulin was used as a loading control. (C) Cell numbers were measured by cell count after the transfection of control shRNA or shEZH2 in SU-DHL-2 cells for the indicated days (left). EZH2 and H3K27me3 levels were measured by western blot assay. H3 and tubulin were used as loading controls (right). (D) Schematic representation of the EZH2 degrader design. (E) Docking conformation of EPZ6438 in the catalytic domain of EZH2 (PDB ID: 5LS6, left) and the chemical structure of EPZ6438 (right). Note: EPZ stands for EPZ6438 in this figure and the following figures.

proteasome for degradation to remove the protein redundancy. Proteolysis targeting chimeras (PROTACs) can achieve selective protein degradation by artificially hijacking natural ubiquitin−proteasome systems. PROTAC-based degraders have two crucial warheads: one binding to a protein of interest (POI) and the other binding to E3 ubiquitin ligase. These special bifunctional molecules force a handshake between an E3 ligase and the POI to artificially ubiquitylate the POI that is subsequently subjected to the proteasome-mediated depletion.[20] The PROTAC technology has been employed to degrade several proteins like BRD4,[21,22] AR,[23] and Stat3.[24] PROTAC-based degraders not only intervene in the enzymatic activities that are targeted by the traditional inhibitors but also disturb nonenzymatic functions of the interested protein, and they may substantially improve the therapeutic efficacy and overcome the inhibitor-mediated drug resistance.[20,25,26] Moreover, the potential advantages of PROTACs in the epigenetic context have also been attracting the attention of researchers. Compared with the parental epigenetic inhibitors, epigenetic PROTACs endowed with higher target selectivity, increased potency, prolonged action, reduced side-effects, and risk of resistance would offer more potential therapeutic strategies for the epigenetic POI-dependent cancers and would be very useful as chemical tools for dissecting the biological roles of the epigenetic POI.[27,28]

Herein, we report the development of specific EZH2 degraders YM181 and YM281 based on PROTAC and further elaborate their better antitumor effects against not only DLBCL but also other types of lymphomas in vitro and in vivo compared to the parental EZH2 inhibitor EPZ6438. Meanwhile, YM281 caused robust cell death and substantial viability inhibition of primary lymphoma cells from patients. Our work provides novel EZH2 degraders to target a broad range of lymphomas of which EZH2 inhibitors only exhibit their limited efficacy to DLBCL.

RESULTS

Design and Screening of EZH2 Degraders via the PROTAC Strategy. In our previous work, we found that the most advanced EZH2 inhibitor EPZ6438 required high doses to reach reasonable in vitro antiproliferative activity against acute myeloid leukemia, although the compound was reported to suppress EZH2 activity largely at nanomolar concentration levels.[16,29] Since lymphomas are believed to be more sensitive to EZH2 inhibitors, EPZ6438 was used to screen our laboratory available lymphoma cell lines, including Burkitt's lymphoma (BL), lymphoblastic lymphoma (LBL), mantle cell lymphoma (MCL), and DLBCL cell lines. However, most lymphoma cell lines and even one DLBCL cell line Toledo did not exhibit obvious responses to EZH2 inhibition, although EZH2 protein levels are similar in all cell lines (Figure 1A,B). Moreover, EPZ6438 could not completely suppress the cell growth of the tested DLBCL (SU-DHL-2, SU-DHL-4, and SU-DHL-6), which are widely reported to be sensitive to EZH2 inhibition, with at least 25% cells remaining viable even at a high dose (10 μM). Meanwhile, the EZH2 knockdown almost completely inhibited the cell growth of SU-DHL-2 (Figure 1C). These observations confirmed the necessity of the development of EZH2 degraders. Using the conventional PROTAC strategy (Figure 1D), our molecular docking model indicated a possibility of the morpholine end to be extended to

https://doi.org/10.1021/acs.jmedchem.1c00460
J. Med. Chem. 2021, 64, 10167−10184

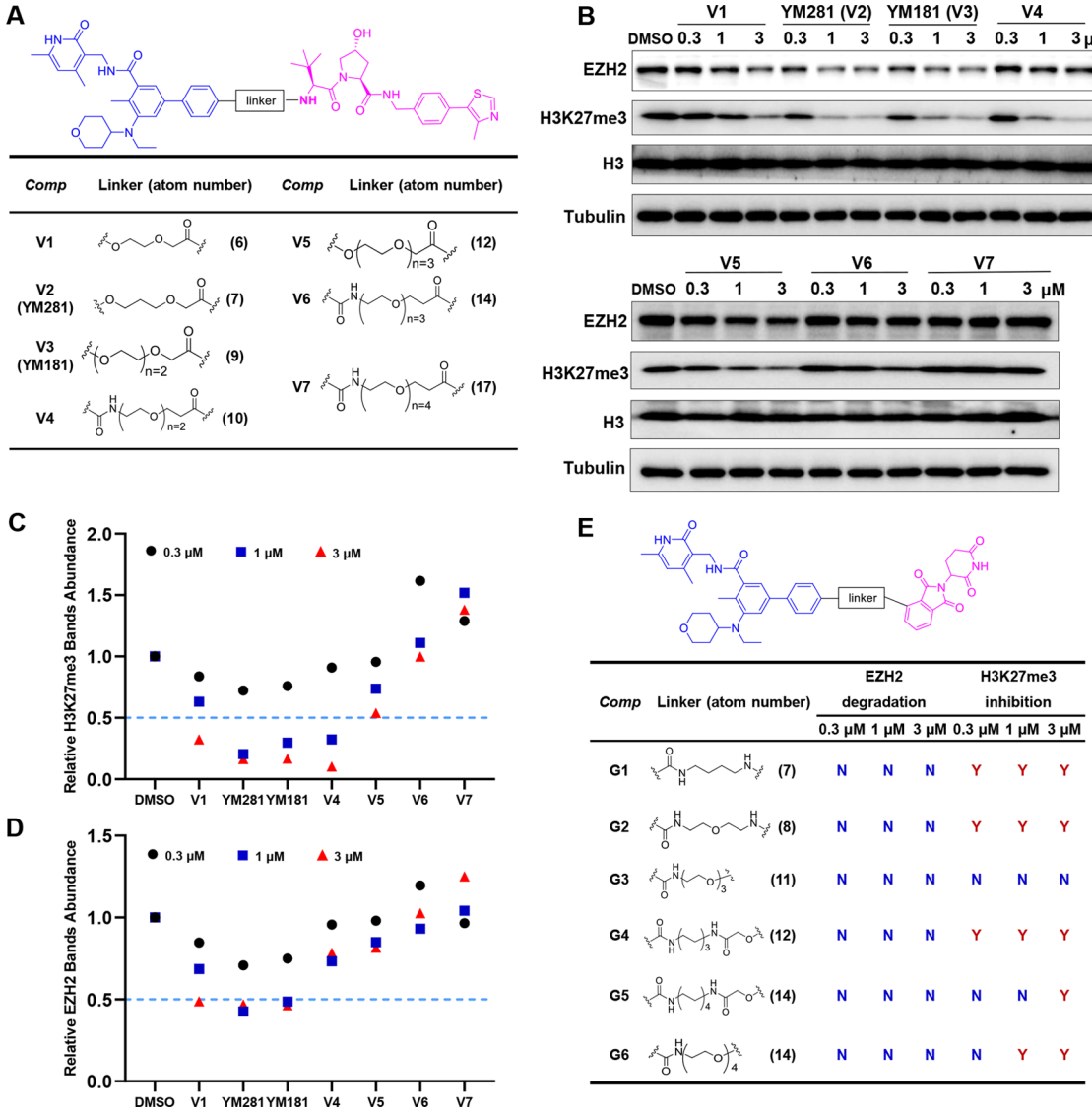

Figure 2. Chemical structures and degradation efficacy of the EZH2 degraders. (A) Chemical structures and linker lengths of VHL-based PROTACs. (B) Western blot analysis of EZH2 and H3K27me3 levels in 22Rv1 cells treated with indicated concentrations of compounds or dimethyl sulfoxide (DMSO) for 48 h. H3 and tubulin were used as loading controls. (C, D) Scatter plots showing the relative (C) H3K27me3 and (D) EZH2 bands abundance in B. (E) Chemical structures and degradation efficiency of CRBN-based PROTACs. N, no significant effects on the related target and Y, significant effects on the related target.

an E3 ligase binder to assemble EZH2 degraders (Figure 1E).[30]

We removed the morpholine motif with a direct linker connected to EPZ6438 to minimize the overall final molecular size for proper cellular permeability. Then, two series of PROTAC-based EZH2 degraders were designed and synthesized to hijack two widely studied E3 ligase systems containing either von Hippel−Lindau (VHL) or cereblon (CRBN). Compounds **V1**−**V7** were linked in different lengths to a small peptide-like fragment that can bind to VHL (Figure 2A).[31,32] Detection of the EZH2 protein level and its catalytic activity mark H3K27me3 by western blot was performed to screen the synthetic compounds at a 0.3−3 μM concentration range to avoid the so-called "hook effect".[33] YM281 (also named as **V2**), YM181 (also named as **V3**), and **V4** significantly decreased the H3K27me3 degree at 1 μM, while **V1** and **V5** required high doses to reach the same level (Figure 2B,C). However, only YM181 and YM281 depleted the half protein level of EZH2 at 1 μM (Figure 2B,D). Neither compound **V6** nor **V7** with a longer linker at either 14 or 17 atoms length had an impact on both levels of EZH2 and H3K27me3, indicating that the over-long linker might sacrifice the binding capacity to EZH2, the cell permeability of compounds, and ternary complex formation. Our second series of designed EZH2 degraders **G1**−**G6** were linked to the thalidomide motif that binds to CRBN. However, none of them showed promising EZH2 degradation capacity, while most of them retained the EZH2 enzymatic inhibition activities (Figures 2E and S1). It seemed that the VHL hijacking approach is more efficient to degrade EZH2.[20] In some cases, a more diverse arsenal of E3 ligase ligands may maximize the opportunity for complementary surfaces between the E3 ligase and POI and thus improve the degradation efficiency of PROTACs.[34−36] Notwithstanding, more investigation is needed to elucidate the exact reason for the failure of G series compounds to degrade EZH2. Based on the EZH2 degradation efficiency, the

https://doi.org/10.1021/acs.jmedchem.1c00460
J. Med. Chem. 2021, 64, 10167−10184

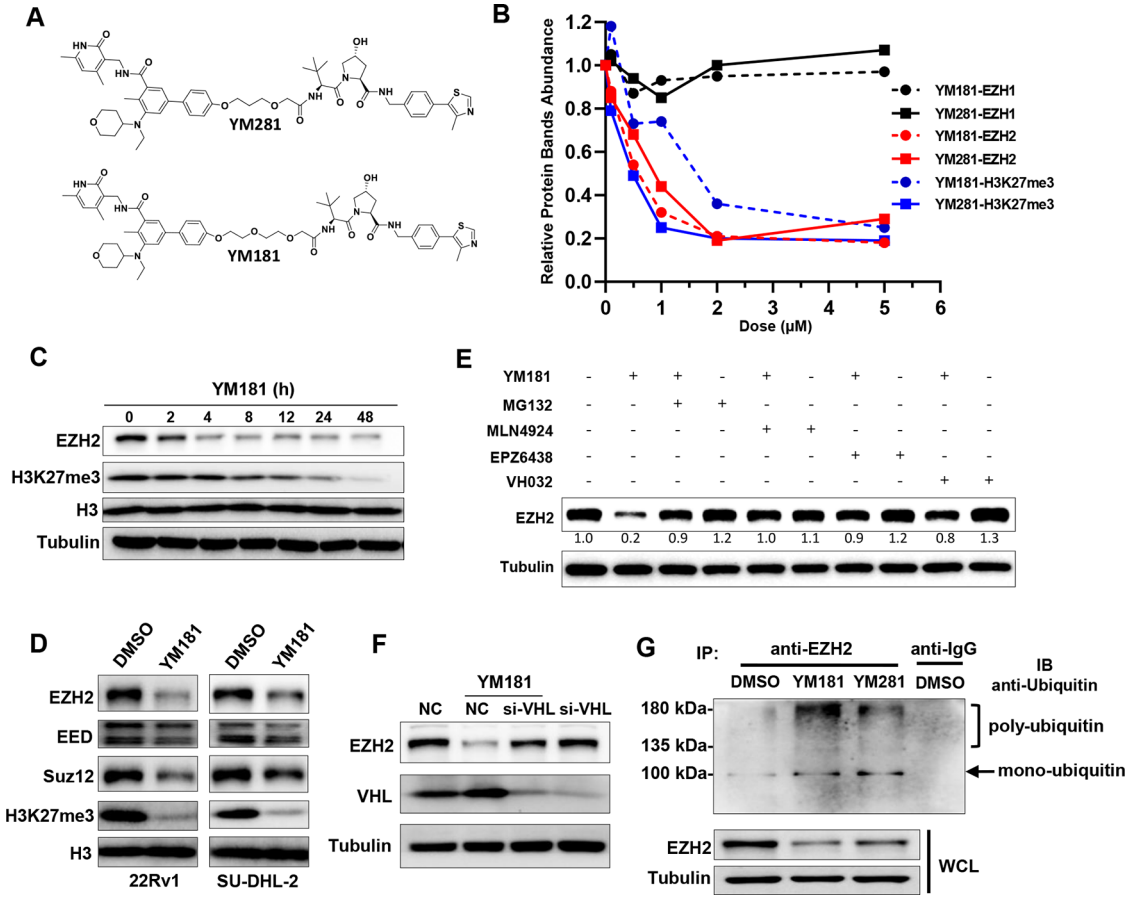

Figure 3. EZH2 degraders abrogated the EZH2 protein level and the PRC2 complex through the VHL-dependent ubiquitin−proteasome system. (A) Chemical structures of YM181 and YM281. (B) Relative protein bands abundance in 22Rv1 cells treated with indicated concentrations of YM181 and YM281 for 24 h. (C) Western blot analysis of EZH2 and H3K27me3 levels in 22Rv1 cells treated with YM181 (2 μM) for the indicated exposure time. H3 and tubulin were used as loading controls. (D) Western blot analysis of the indicated protein levels in 22Rv1 and SU-DHL-2 cells treated with YM181 (2 μM) for 24 h. H3 was used as a loading control. (E) Western blot analysis of EZH2 levels in 22Rv1 cells treated with YM181 (2 μM) for 24 h after 2 h pretreatment with DMSO, MG132 (0.5 μM), MLN-4924 (0.4 μM), EPZ6438 (2 μM), and VH032 (2 μM). Tubulin was used as a loading control. (F) Western blot analysis of EZH2 and VHL levels after the transfection of nontargeting (NC) or VHL siRNAs for 48 h, followed by a 24 h YM181 treatment (2 μM) in 22Rv1 cells. Tubulin was used as a loading control. (G) Immunoprecipitation-western blot analysis of ubiquitylated EZH2 levels in 22Rv1 cells treated with 2 μM YM181 and YM281 for 12 h. Tubulin was used as a loading control.

two best compounds, YM181 and YM281, were chosen for further investigation.

YM181 and YM281 Degraded the EZH2 Protein through the VHL-Dependent Ubiquitin−Proteasome System. As shown in Figure 3A, YM181 and YM281 abrogated both the EZH2 protein level and the H3K27me3 degree in a concentration-dependent manner in 24 h, and moreover had no significant effect on the protein level of EZH1 that is homologous to EZH2 (Figures 3B and S2). The maximum degradation efficacy reached 80% at a concentration of 2 μM. A time-course study demonstrated that the EZH2 degradation could be detected in 2 h, and this effect reached a maximum in 4 h (Figure 3C). It is reported that the PRC2 complex collapse in the absence of any core subunit.[6] To test the influence of EZH2 degraders on the PRC2 complex, the protein levels of the other two subunits, EED and SUZ12, were examined in both SU-DHL-2 and 22Rv1 cells treated with YM181 at 2 μM (Figure 3D). Within 24 h, YM181 substantially reduced the levels of EED and SUZ12. The results demonstrated that YM181 and YM281 rapidly deleted the EZH2 protein and consequently destabilized the PRC2 complex due to the loss of integrity.[25,37,38] Alternatively, it is also possible that EED and/or SUZ12 in proximity to EZH2 may be ubiquitinated by the EZH2-PROTAC-mediated ternary complex formation.[37,38] In the following experiments, as shown in Figure 3E, the degradation effect of YM181 could be rescued by adding either a proteasome inhibitor MG132 or MLN-4924, an inhibitor of the neddylation that is essential to activate the VHL E3 ligase system.[39] Meanwhile, the EZH2 inhibitor EPZ6438 competed with YM181 to occupy the catalytic pocket and subsequently prevented protein degradation. Furthermore, the addition of a synthetic VHL ligand VH032 also reversed the EZH2 degradation caused by YM181. To further confirm the requirement of VHL for YM181-induced EZH2 degradation, VHL was knocked down by siRNAs in 22Rv1 cells. The exposure of the VHL knockdown cells to YM181 did not reduce the EZH2 protein level that was largely degraded in the control cells (Figure 3F). Additionally, Co-IP experiments clearly displayed a significant increase of EZH2 ubiquitination mediated by both YM181 and YM281, while the whole protein level was decreased within 12 h (Figure 3G). These results confirmed that the degradation of

https://doi.org/10.1021/acs.jmedchem.1c00460
J. Med. Chem. 2021, 64, 10167−10184

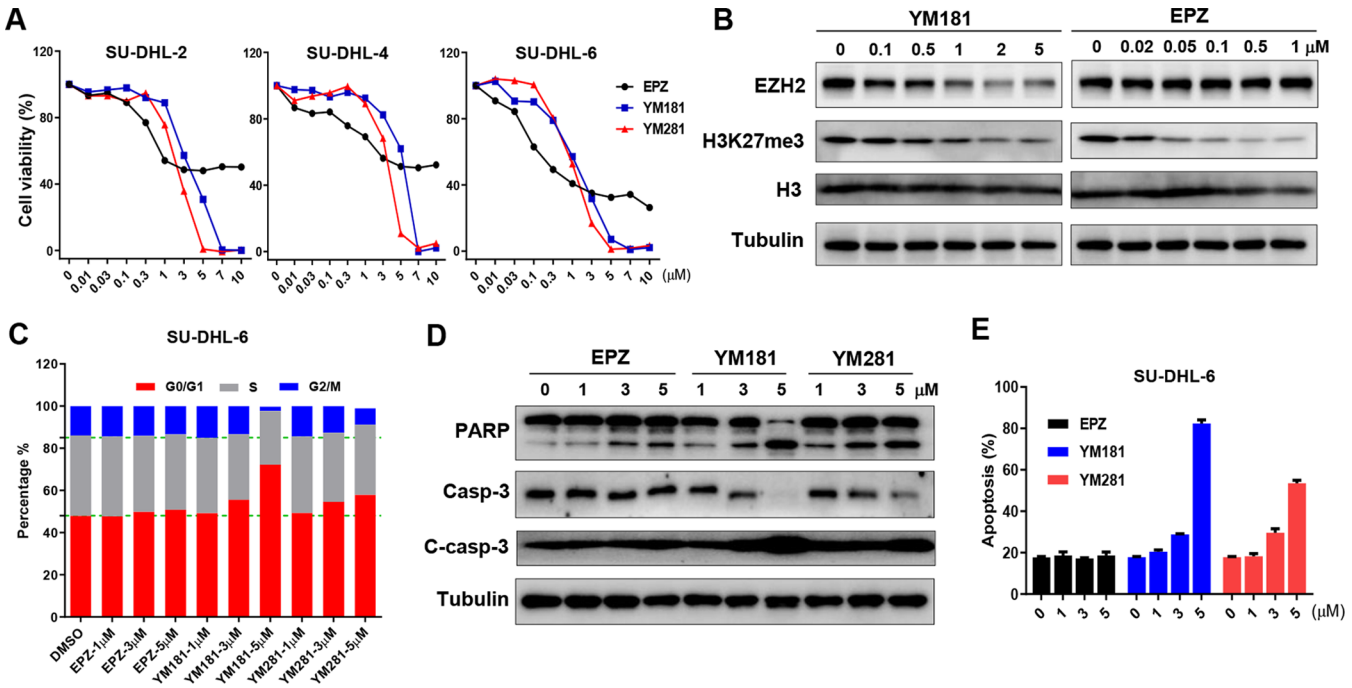

Figure 4. EZH2 degraders displayed stronger anticancer abilities than EPZ6438 in lymphoma cell lines. (A) MTS cell viability curves in different DLBCL cell lines treated with indicated compounds for 5 days. (B) Western blot analysis of EZH2 and H3K27me3 levels in SU-DHL-2 cells treated with the indicated compounds for 24 h. H3 and tubulin were used as loading controls. (C) Cell cycle analysis in SU-DHL-6 cells treated with DMSO or indicated compounds for 24 h. (D) Western blot analysis of PARP, caspase-3, and cleaved-caspase-3 levels in SU-DHL-6 cells treated with indicated compounds for 48 h. Tubulin was used as a loading control. (E) Proportions of PI^+ and/or Annexin-V^+ apoptotic cells in SU-DHL-6 cells treated with indicated compounds for 48 h as measured by flow cytometry.

EZH2 induced by the two compounds was indeed associated with the VHL-dependent ubiquitin−proteasome system.

EZH2 Degraders Displayed Stronger Anticancer Effects than EPZ6438 in Lymphoma Cell Lines. Given that EZH2 inhibitors are reportedly effective in the intervention of DLBCL, anticancer effects of EZH2 degraders were first tested in three DLBCL cell lines, SU-DHL-2, SU-DHL-4, and SU-DHL-6. The MTS assays confirmed that both YM181 and YM281 caused cell viability to decrease stronger than EPZ6438 in all three cell lines (Figure 4A). YM181 and YM281 could induce nearly complete cell viability inhibition compared to EPZ6438, although their initial effective concentrations were slightly higher. Meanwhile, EPZ6438 only achieved half inhibition in SU-DHL-2 and SU-DHL-4 cells and 70% inhibition in SU-DHL-6. Moreover, all of the other lymphoma cell lines that were resistant to the EZH2 inhibitor also showed a complete response to the EZH2 degraders (Figure S3A). Western blot analysis further confirmed that YM181 induced substantial EZH2 degradation (Figures 4B and S3B,C). EPZ6438 robustly reduced the H3K27me3 levels at low nanomolar concentrations, while YM181 required high doses. The installment of both the linker and the VHL ligand motif might cause an EZH2 inhibitory activity loss, explaining the reason why EZH2 degraders needed a higher effect-starting concentration. To study whether the linker and the VHL ligand warhead would bring off-target effects, we also evaluated the cytostatic effects of V6 and V7 that are structurally similar but do not induce EZH2 degradation. Neither V6 nor V7 induced significant cell viability inhibition (Figure S3D,E). Meanwhile, we synthesized YM620, an isomer of YM281, with alterations of two stereocenters in hydroxyproline, which diminish the binding affinity to VHL (Figure S3F). Indeed, YM620 did not have an apparent effect on the EZH2 protein level, while it substantially inhibited EZH2 enzymatic activity (Figure S3G). Compared to YM281, YM620 had a weaker antiproliferative capacity in two tested cancer cell lines (Figure S3H). All of these data excluded the off-target effects of our EZH2 degraders.

To investigate how the EZH2 degraders intervene in cell growth of lymphoma cells, both the cell cycle and apoptosis analyses were conducted. After a 24 h treatment, EZP6438 at the tested doses (1, 3, 5 μM) slightly caused a G0/G1 phase arrest of SU-DHL-6 cells without significant observation of sub-G1 increase (Figures 4C and S4A). However, YM181 and YM281 at the same doses led to a concentration-dependent cell cycle arrest and a profound sub-G1 population increase. The caspase-3/7 assay demonstrated that EZH2 degraders increased the activity of caspase-3/7, and western blot also showed that the cleaved caspase-3 and PARP were significantly increased, indicating the apoptotic event (Figures 4D and S4B,C). The Annexin-V/PI assay further verified that apoptosis was clearly induced by both EZH2 degraders in a dose-dependent manner, while EZP6438 did not (Figures 4E and S4D). These results demonstrated that EZH2 degraders induced obvious cell cycle arrest and apoptosis, which might be the reasons why YM181 and YM281 could achieve a complete cell viability inhibition, whereas EPZ6438 could not if only inhibiting the methylation function of EZH2.

EZH2 Degraders Reduced Tumor Growth In Vivo and Decreased Cell Viability in Primary Lymphoma Patient Cells. To investigate the antitumor activity of EZH2 degraders in vivo, a xenograft mouse model of DLBCL cell line SU-DHL-6 was first conducted. Consistent with in vitro results, YM281 (80 mg/kg) administered by intraperitoneal injection 6 times

https://doi.org/10.1021/acs.jmedchem.1c00460
J. Med. Chem. 2021, 64, 10167−10184

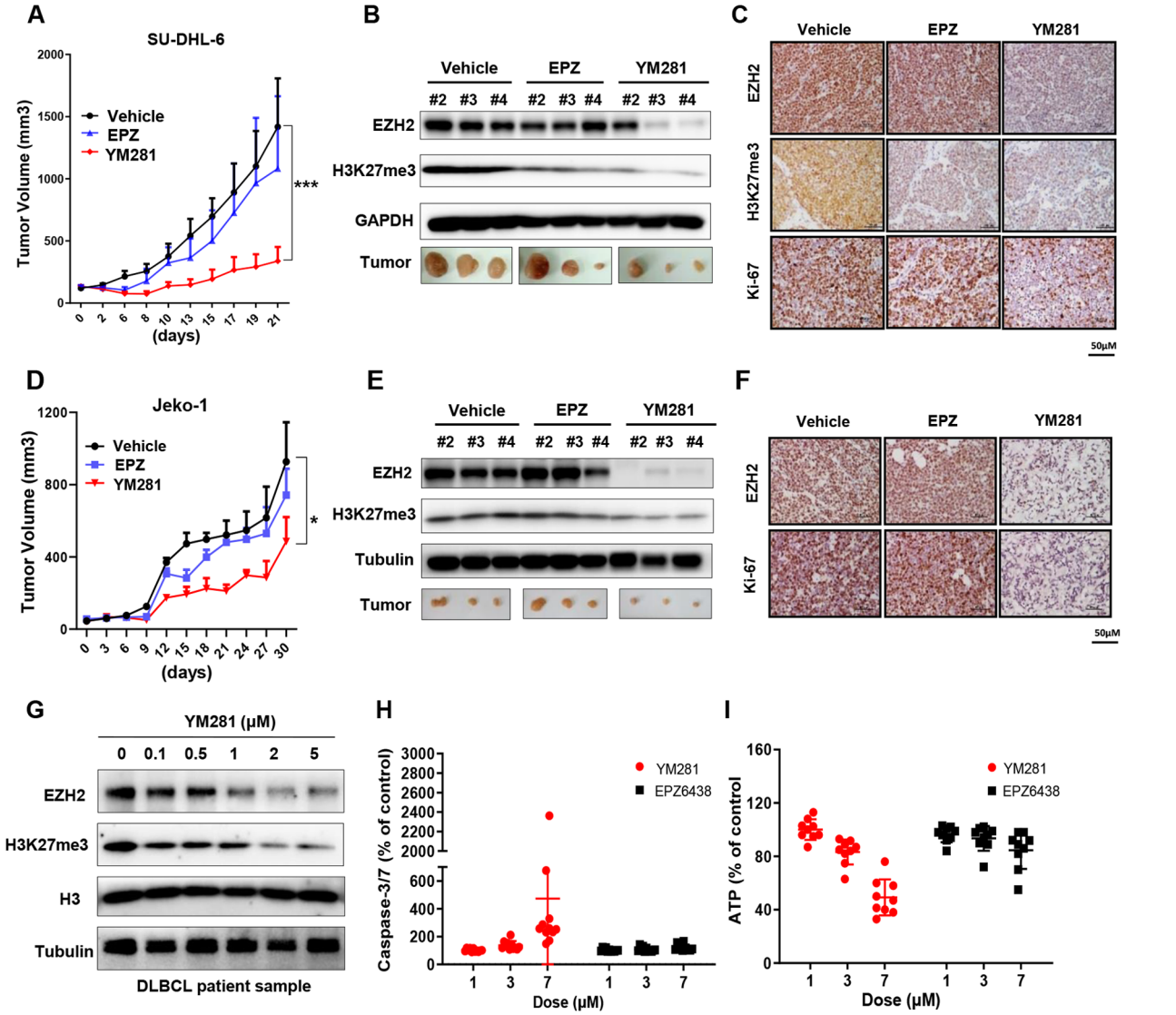

Figure 5. EZH2 degraders reduced tumor growth in vivo and decreased cell viability in primary lymphoma patient cells. (A) Tumor volume of Balb/c nude mice bearing SU-DHL-6 xenograft administrated intraperitoneally with a vehicle, YM281 (80 mg/kg) or EPZ (42.5 mg/kg), for 3 weeks. (B) Western blot analysis of EZH2 and H3K27me3 levels in the representative SU-DHL-6 model excised tumors. GAPDH was used as a loading control. Representative tumor images were presented. (C) Immunohistochemistry analysis of EZH2, H3K27me3, and Ki67 levels in the representative excised tumors from A. (D) Tumor volume of Balb/c nude mice bearing the Jeko-1 xenograft administrated intraperitoneally with a vehicle, YM281 (100 mg/kg) or EPZ (50 mg/kg), for 30 days. (E) Western blot analysis of EZH2 and H3K27me3 in the representative Jeko-1 model excised tumors. Tubulin was used as a loading control. Representative tumor images were presented. (F) Immunohistochemistry analysis of EZH2 and Ki67 levels in the representative Jeko-1 model excised tumors. (G) Western blot analysis of EZH2 and H3K27me3 levels in a DLBCL patient sample's cells treated with YM281 at indicated concentrations for 24 h. H3 and tubulin were used as loading controls. (H) Caspase-3/7 activity of patient-derived primary lymphoma cells treated with each compound at indicated concentrations for 48 h in 11 lymphoma patient cases. (I) Quantitation of the present ATP level in patient-derived cells with each compound at indicated concentrations for 48 h in 11 lymphoma patient cases.

weekly for 3 weeks remarkably suppressed the tumor volume (Figure 5A). However, EPZ6438 at the equal molar dose to YM281 (42.5 mg/kg) failed. Neither EPZ6438 nor YM281 caused significant weight loss in mice (Figure S5A). Western blot analysis of tumor tissue showed that YM281 significantly reduced the EZH2 protein and H3K27me3 levels (Figure 5B). EPZ36438 did not prevent the tumor growth, although it substantially decreased the H3K27me3 level, indicating that the enzymatic inhibition of EZH2 might not be enough to attenuate lymphoma cells in vivo. The significant destabilization of EZH2 and inhibition of tumor proliferation (indicated by Ki67 staining) induced by YM281 was further confirmed by immunohistochemistry in the tumor slices (Figure 5C). The in vivo anticancer efficacy in DLBCL was validated in the mice xenograft model of Jeko-1, a mantle cell lymphoma cell line (Figures 5D–F and S5B). More importantly, the tumor weight was clearly associated with the EZH2 protein level in YM281 treated mice (Figure S5C,D). Finally, to evaluate the potential clinical implication of EZH2 degraders that showed promising efficacy in all different lymphoma cell lines, as shown in Figure S3A, primary lymphoma cells extracted from various lymphoma patient samples were used for further tests. First, EZH2 degrader YM281 induced dose-dependent EZH2 degradation in primary cells from one DLBCL patient (Figure

https://doi.org/10.1021/acs.jmedchem.1c00460
J. Med. Chem. 2021, 64, 10167−10184

Scheme 1. Synthesis of Intermediate Compounds 6 and 7[a]

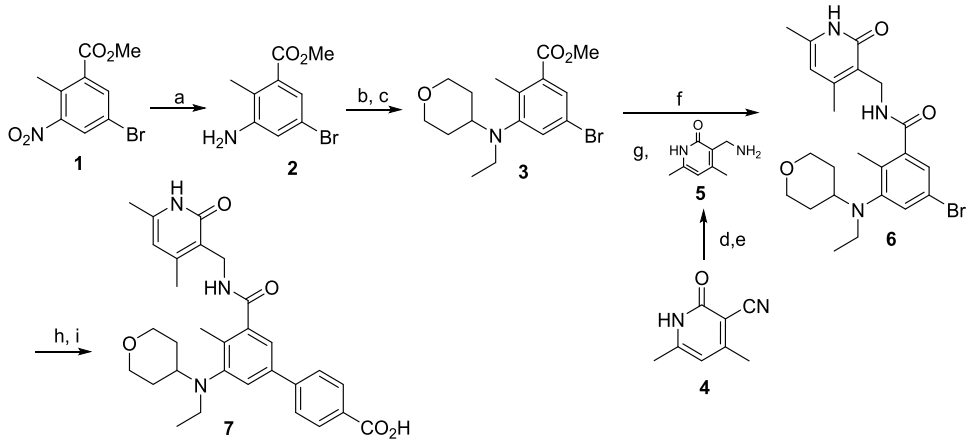

[a]Reagents and conditions: (a) Fe, NH_4Cl, MeOH, 90 °C; (b) tetrahydro-4*H*-pyran-4-one, AcOH, $Na(AcO)_3BH$, 1,2-dichloroethane; (c) acetaldehyde, AcOH, $Na(AcO)_3BH$, 1,2-dichloroethane; (d) Boc_2O, H_2, Raney-Ni, MeOH; (e) HCl/MeOH; (f) NaOH, EtOH, 60 °C; (g) HOBt, EDCI, NMM, DMSO; (h) 4-methoxycarbonylphenylboronic acid, K_2CO_3, $Pd(PPh_3)_4$, *N*,*N*-dimethylformamide (DMF), 90 °C; and (i) NaOH, EtOH, 60 °C. Note: unless stated, reactions underwent at room temperature in all synthetic schemes.

Scheme 2. Synthesis of VHL Ligands 15, 16, and VH032[a]

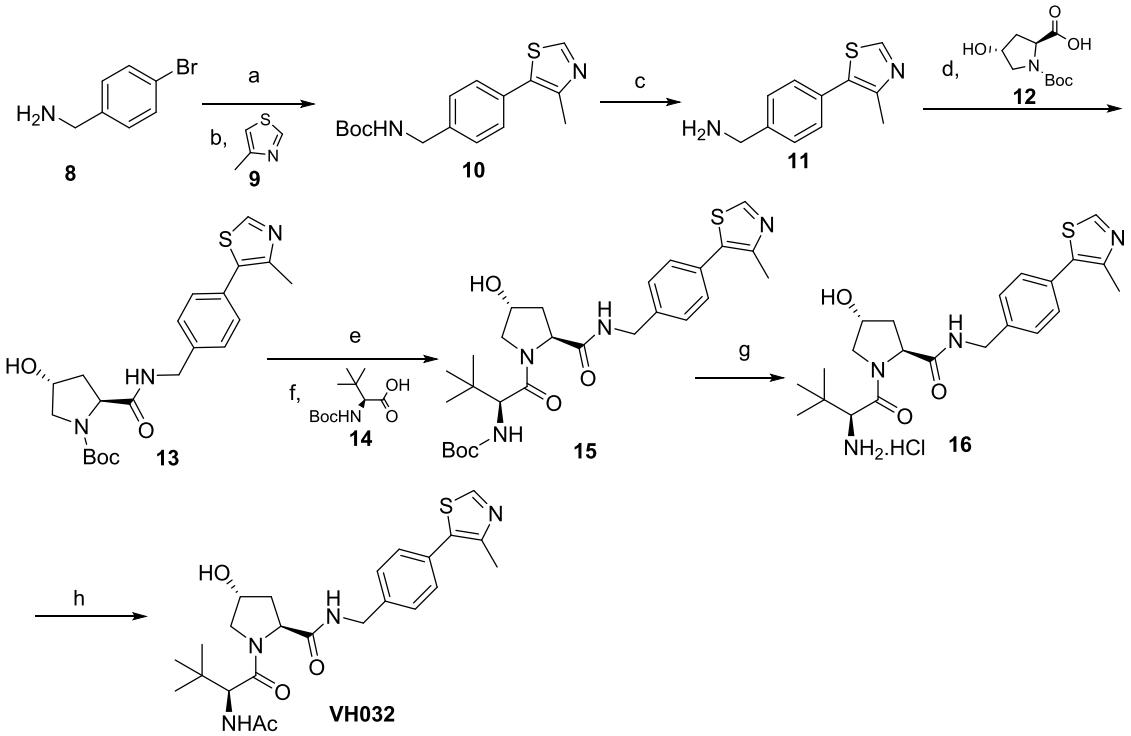

[a]Reagents and conditions: (a) NaOH, Boc_2O, MeOH; (b) $Pd(OAc)_2$, KOAc, *N*,*N*-dimethylacetamide (DMA), 150 °C; (c) HCl/MeOH; (d) **12**, HATU, *N*,*N*-diisopropylethylamine (DIPEA), tetrahydrofuran (THF); (e) HCl/MeOH; (f) **14**, HATU, DIPEA, DMF; (g) HCl/MeOH; and (h) DIPEA, acetic anhydride, CH_2Cl_2.

5G and Table S1). Furthermore, lymphoma primary cells from 11 cases of lymphoma patients, including two cases of BLBCL, were tested for the efficacy of YM281. Compared to EPZ6438, YM281 increased the activity of caspase-3 and -7 and meanwhile reduced the cell viability observed in adenosine triphosphate (ATP) assays (Figure 5H,I).

CHEMISTRY

The synthesis of the key intermediates **6**, **7**, VHL ligands **16** and VH032, and CRBN ligands **32** and **33** have been previously described (Schemes 1, 2, and 5).[31,40−43] As shown in Scheme 3, compound **V2** (YM281) was used as an example for the synthesis of series V compounds. The commercially available propane-1,3-diol (**17b**) was protected by the benzyl group on one side hydroxyl and then reacted with *t*-butyl bromoacetate. The removal of the benzyl group under catalytic hydrogenation conditions followed by a substitution reaction of hydroxyl with tosyl chloride gave compound **19b**. Alkylation of 4-hydroxyphenylboronic acid pinacol ester with **19b** afforded **20b**, and consequential Suzuki coupling with

https://doi.org/10.1021/acs.jmedchem.1c00460
J. Med. Chem. 2021, 64, 10167−10184

Scheme 3. Synthesis of Series V Compounds[a]

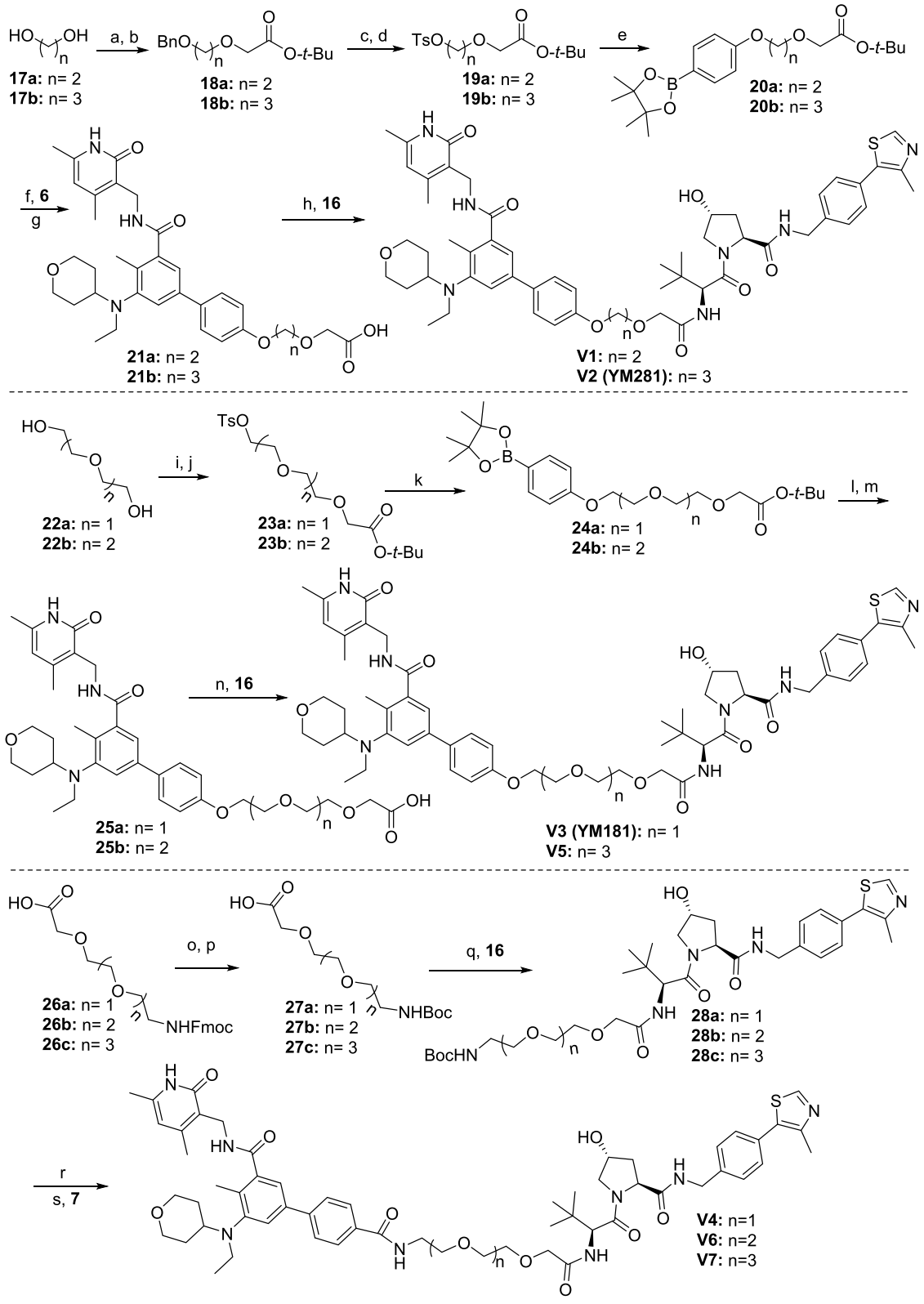

[a]Reagents and conditions: (a) BnBr, NaH, THF; (b) *tert*-butyl bromoacetate, NaOH, TBACl, CH_2Cl_2; (c) Pd/C, H_2, EtOH; (d) TsCl, DMAP, TEA, CH_2Cl_2; (e) 4-hydroxyphenylboronic acid pinacol ester, K_2CO_3, DMF, 70 °C; (f) **6**, K_3PO_4, $Pd(PPh)_4$, DMF, 90 °C; (g) 20% TFA, CH_2Cl_2; (h) **16**, HATU, DIPEA, DMF; (i) NaH, *tert*-butyl bromoacetate, DMF; (j) TsCl, DMAP, TEA, CH_2Cl_2; (k) 4-hydroxyphenylboronic acid pinacol ester, K_2CO_3, DMF, 70 °C; (l) **6**, K_3PO_4, $Pd(PPh)_4$, DMF, 90 °C; (m) 20% TFA, CH_2Cl_2; (n) **16**, HATU, DIPEA, DMF; (o) diethylamine, CH_2Cl_2; (p) Boc_2O, NaOH, CH_2Cl_2; (q) **16**, HATU, DIPEA, DMF; (r) HCl/MeOH; and (s) **7**, HATU, DIPEA, DMF.

https://doi.org/10.1021/acs.jmedchem.1c00460
J. Med. Chem. 2021, 64, 10167−10184

Scheme 4. Synthesis of YM620[a]

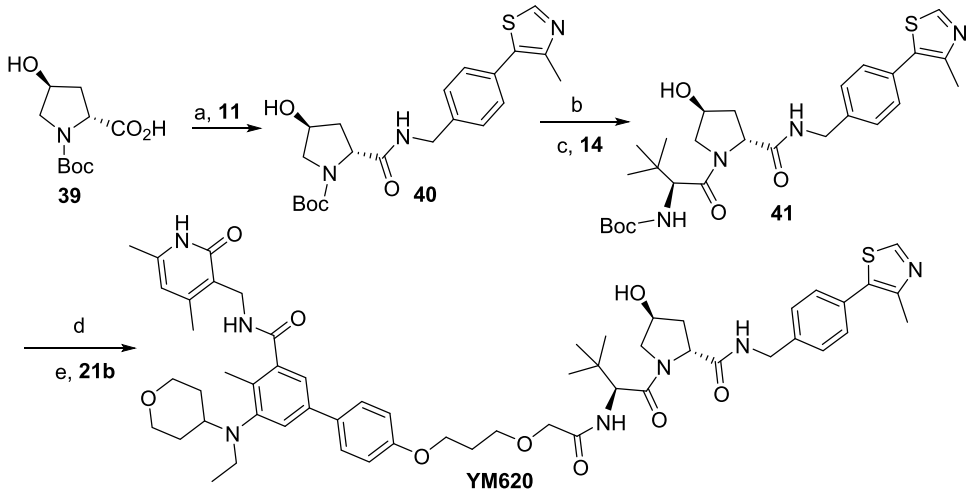

[a]Reagents and conditions: (a) **11**, HATU, DIPEA, THF; (b) HCl/MeOH; (c) **14**, HATU, DIPEA; (d) HCl/MeOH; and (e) **21b**, HATU, DIPEA, DMF.

compound **6** and the removal of the Boc group under acidic conditions gave the acid **21b**. The final compound **V2** (YM281) was obtained via standard amide coupling between acid **21b** and the amine **16**. In a similar manner, other V series compounds **V1**, **V3** (YM181), **V4**-**V7**, and YM620 modified with the varying linker were prepared, as shown in Schemes 3 and 4.

Compound **G5** was used as an example for the synthesis of series G compounds (Scheme 5). The commercially available octane-1,8-diamine was protected by Boc on one side amine to give **37b**. Amide coupling with **36**[41] and subsequent removal of the Boc group under acidic conditions afforded amine **38b**. The final compound **G5** was obtained via standard amide coupling between acid **7** and amine **38b**. In a similar manner, other series G compound **G1**−**G4** and **G6** modified with the varying linker were prepared.

DISCUSSION AND CONCLUSION

As widely conceptualized, EZH2 inhibitors that simply suppress EZH2 enzymatic activity exhibit antitumor effects by inhibiting trimethylation of H3K27 and thereby activating tumor suppressor genes.[6,7] This class of EZH2 inhibitors reduces H3K27 methylation levels at very low concentrations. However, their therapeutic efficacy varies largely in different types of tumors; for example, DLBCL is the major subtype of lymphomas that are most sensitive to EZH2 inhibitors. Previous research studies indicated that the whole EZH2 protein itself is involved in tumor proliferation.[5,10,16,17] Therefore, abrogating the whole EZH2 protein may have a significant therapeutic advantage over simply inhibiting its enzymatic activity. Chen and co-workers have reported that gambogenic acid derivatives could covalently bind to Cys668 within the EZH2-SET domain, triggering EZH2 degradation to inhibit head and neck cancer cells.[44] But the selectivity of gambogenic acid derivatives for EZH2 is questionable.[45] Very recently, Jin's group reported a hydrophobic tagging-based EZH2 degrader (MS1943) that showed better anticancer capacity in triple-negative breast cancer than the parental EZH2 inhibitor.[46] Surprisingly, MS1943 was reported to reduce the protein level of SUZ12 without affecting the EED protein level, which is different from our EZH2 PROTACs that reduce the EED protein level as well.[46] The concomitant degradation of EED induced by YM281 and YM181 could either result from collateral ubiquitination of EED by the VHL E3 ligase due to its proximity to EZH2 or from the reduced stability of the PRC2 complex to eject the EED subunit after the first EZH2 degradation.[25,39,47] The exact mechanism remains to be elucidated in the future. More recently, some CRBN-based PROTACs were reported while our revised manuscript was under review.[48] However, their compounds remained to be evaluated in the animal study. Meanwhile, PROTAC-based degradation of EED, another subunit of the PRC2 complex, was also reported recently.[37,38] However, the reported EED degraders did not show superior in vitro anticancer activities compared with their parental EED inhibitors, whereas more in vivo experiments are also needed to validate their efficacy.

In our observation, the therapeutic efficacy of EZH2 inhibitors was limited to DLBCL cell lines among the tested lymphoma cell lines (Figure 1A). We wonder whether the direct EZH2 degradation via PROTAC technology could be developed to improve their targeting capacity to the other types of lymphoma cells. In our current study, we developed PROTAC-based EZH2 degraders and investigated their efficiency of EZH2 degradation and therapeutic efficacy in various types of lymphoma in vitro and in vivo. Our study revealed that only VHL-targeting compounds enabled the EZH2 degradation with an appropriate linker at 7 or 9 atoms length. Compared to the parental EZH2 inhibitor EPZ6438, our two best EZH2 degraders YM181 and YM281 selectively degraded EZH2 over EZH1, and they exhibited effective antiproliferative activity both in DLBCL and other types of lymphoma cell lines. Furthermore, the EZH2 degrader showed an apparent advantage to prevent in vivo tumor growth in lymphoma xenografts without obvious toxicity at the efficacious doses.

However, the incomplete EZH2 degradation and the modest cellular potencies for YM281 and YM181 in the inhibition of cell viability at low concentrations suggest that there is still room for further optimization. In the future, a structure and activity relationship study on different linker scaffoldings with the same linking length as YM181 and YM281 may be

https://doi.org/10.1021/acs.jmedchem.1c00460
J. Med. Chem. 2021, 64, 10167−10184

Scheme 5. Synthesis of Series G Compounds[a]

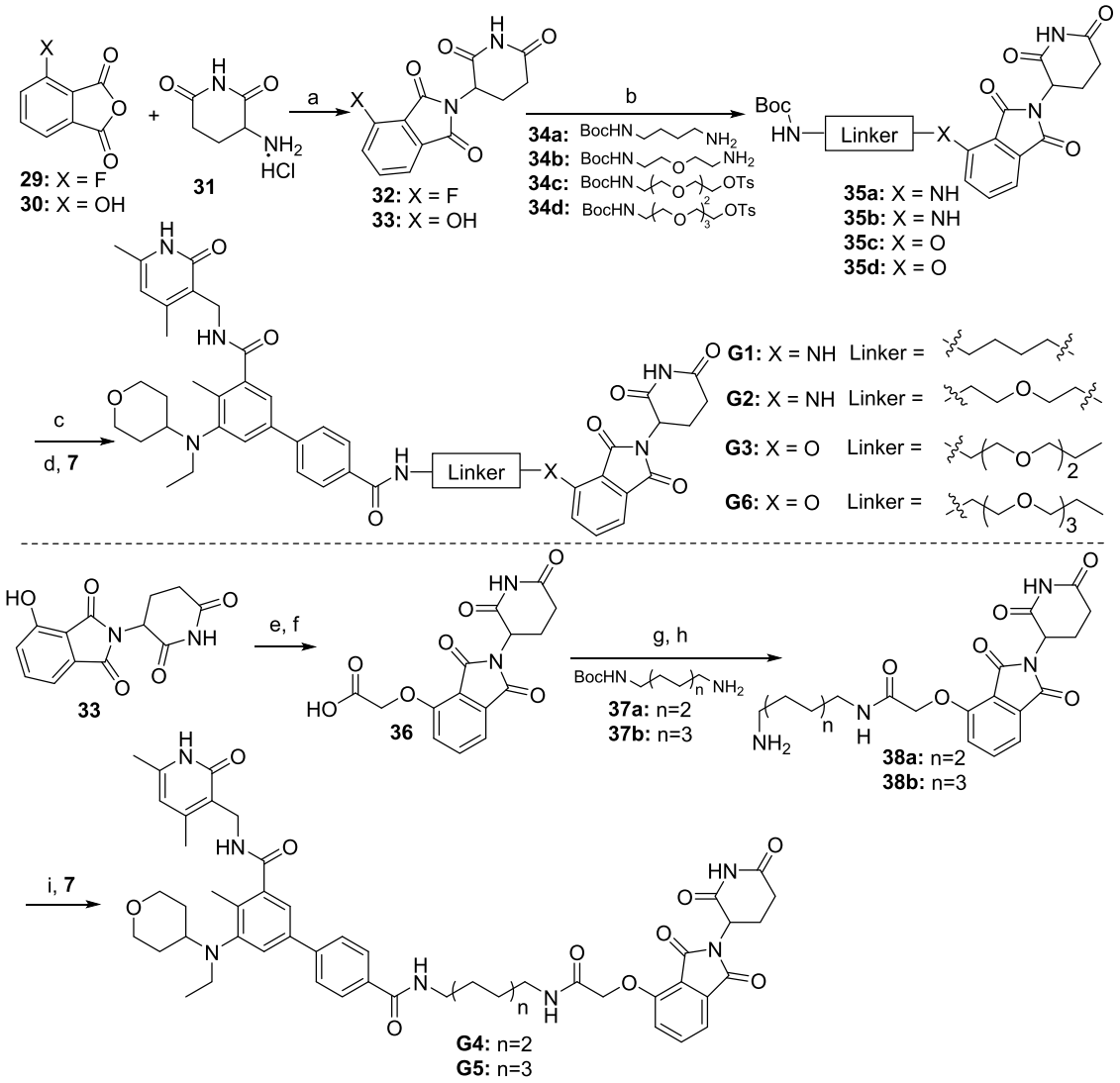

[a]Reagents and conditions: (a) **29**, NaOAc, AcOH, 120 °C reflux, or **30**, pyridine, 110 °C; (b) **34a−b**, DIPEA, DMF 90 °C or **34c−d**, Na_2CO_3, DMF, 80 °C; (c) 20% TFA, CH_2Cl_2; (d) **7**, HATU, DIPEA, DMF; (e) *tert*-butyl bromoacetate, K_2CO_3, DMF; (f) 20% TFA, CH_2Cl_2; (g) HATU, DIPEA, DMF; (h) 20% TFA, CH_2Cl_2, 50 °C; and (i) **7**, HATU, DIPEA, DMF.

warranted to obtain more potent EZH2 degraders. Meanwhile, cancer cells that may not depend on EZH2 for their tumorigenesis, for example, pancreatic cancer cell AsPC1 and lung cancer cell NCI-H460, are not sensitive to YM181 and YM181, although the compounds were able to decrease their EZH2 levels (Figure S6). By measuring cell permeability with Caco-2 cells, both YM181 and YM281 showed their apparent permeability ability largely compromised compared to the parental EHZ2 inhibitor EPZ6438 (Table S2), indicating the importance to improve their oral bioavailability through further structural optimization. Overall, our results demonstrate that EZH2 degraders may have better therapeutic potential than EZH2 inhibitors against lymphomas. The exact mechanism of action and the application of our EZH2 degraders in other cancers are under investigation.

EXPERIMENTAL SECTION

Chemistry: General Experiment and Information. Synthesis details for the key final compounds are described here. All solvents were commercially available and were used without further purification unless stated. The chemicals used were either purchased from commercial sources or prepared according to literature procedures. The ^1H and ^{13}C nuclear magnetic resonance (NMR) spectra were recorded on a Bruker Avance spectrometer 400 at 400 MHz and 100 MHz or a Bruker Avance spectrometer 500 at 500 MHz and 125 MHz respectively. Chemical shifts are given in ppm (δ) referenced to $CDCl_3$ with 7.26 for ^1H and 77.10 for ^{13}C, and to d_6-DMSO with 2.50 for ^1H and 39.5 for ^{13}C. In the case of multiplet, the signals are reported as intervals. Signals are abbreviated as follows: s, singlet; d, doublet; t, triplet; q, quartet; and m, multiplet. Coupling constants are expressed in hertz. High-resolution mass spectra (HRMS) were recorded on a BRUKER VPEXII spectrometer (the ESI mode). The progress of the reactions was monitored by thin-layer chromatography on a glass plate coated with silica gel with a fluorescent indicator (GF254). Flash column chromatography was performed on silica gel (200−300 mesh). An Agilent 1100 HPLC system equipped with an Eclipse XDB-C18 column was used to determine the purity of all of the final key products. Gradient elution: 10−90% MeOH against H_2O with 0.1% TFA over 15 min (the ratio of MeOH/H_2O from 10 to 90% in 8 min, and finally 90% for 7 min) at a flow rate of 1.0 mL/min; detection wavelength: 254 nm. All biologically tested compounds had a purity of more than 95%.

https://doi.org/10.1021/acs.jmedchem.1c00460
J. Med. Chem. 2021, 64, 10167−10184

*5-Bromo-N-((4,6-dimethyl-2-oxo-1,2-dihydropyridin-3-yl)-methyl)-3-(ethyl(tetrahydro-2H-pyran-4-yl)amino)-2-methylbenzamide (**6**).*[40] To a solution of methyl 5-bromo-2-methyl-3-nitrobenzoate (5 g, 18.24 mmol) in MeOH (50 mL), Fe (5.09 g, 91.22 mmol) and NH_4Cl (1.95 g, 36.49 mmol) were added sequentially. The mixture was stirred at 90 °C overnight. In the end, the solid precipitated was filtered off and washed with MeOH (3 × 80 mL). The combined filtrate was dried and concentrated under reduced pressure to give the desired crude **2** as a yellow liquid (4.34 g, 99.6% yield). To a solution of **2** (4.34 g, 17.78 mmol) in 1,2-dichloroethane (50 mL) were added tetrahydro-4*H*-pyran-4-one (2.46 mL, 26.67 mmol) and AcOH (6.10 mL, 106.68 mmol). The mixture was stirred at r.t. for 0.5 h before $Na(AcO)_3BH$ (11.31 g, 53.34 mmol) was added at 0 °C. The mixture was warmed to r.t. and stirred for 24 h. EtOAc and water were added, and the aqueous phase was extracted with EtOAc twice. The combined organic phases were dried over Na_2SO_4, filtered, and concentrated under reduced pressure. The residue was purified by flash column chromatography with EtOAc/PE (10−35%) to afford the product as a yellow solid (5.34 g, 91.5% yield). To a solution of the product (5.34 g, 16.27 mmol) in 1,2-dichloroethane (50 mL) were added acetaldehyde (2.76 mL, 48.81 mmol) and AcOH (5.58 mL, 97.62 mmol). The mixture was stirred at r.t. for 0.5 h before $Na(AcO)_3BH$ (10.35 g, 48.81 mmol) was added at 0 °C. The mixture was warmed to r.t. and stirred for 24 h before EtOAc (200 mL) and water (100 mL) were added. The aqueous layer was extracted with EtOAc (2 × 150 mL). The combined organic phases were dried over Na_2SO_4, filtered, and concentrated under reduced pressure. The residue was purified by flash column chromatography with EtOAc/PE (10−35%) to afford **3** as a yellow solid (5.18 g, 89.4% yield).

To a solution of 4,6-dimethyl-2-oxo-1,2-dihydro-3-pyridinecarbonitrile **4** (3.0 g, 20.25 mmol) in MeOH (120 mL) was added a catalytic amount of Raney nickel and Boc_2O (5.3 g, 24.30 mmol). The mixture was purged and refilled with H_2 three times and stirred at r.t. for 12 h under H_2. After filtration and concentration, the residue was purified by flash column chromatography with $MeOH/CH_2Cl_2$ (2−5%) to afford a white solid (5.1 g, 99.6% yield). Acetyl chloride (5.74 mL, 80.68 mmol) was added to MeOH (28 mL) at 0 °C for 1 h to prepare a fresh HCl solution in methanol, and then the above-obtained compound (5.09 g, 20.17 mmol) was added. The solution was warmed to r.t., stirred for 3 h, and finally concentrated under reduced pressure to give **5** (4.1 g, 100% yield) without further purification.

To a solution of **3** (5.18 g, 14.54 mmol) in ethanol (50 mL) was added aqueous NaOH solution. The reaction mixture was stirred at 60 °C for 3 h before it was concentrated under reduced pressure. Then, CH_2Cl_2 (100 mL) and water (150 mL) were added, and the mixture was washed with CH_2Cl_2 (2 × 100 mL). The aqueous phase was acidified by adding aq. HCl (1 M) until pH = 3−4. Then, the aqueous solution was extracted with CH_2Cl_2 (3 × 200 mL). The combined organic phases were concentrated under reduced pressure to give the intermediate acid as a white solid (4.55 g, 91.4% yield).

To a solution of **5** (3.03 g, 19.93 mmol) and the above-obtained acid (4.55 g, 13.29 mmol) in DMSO (50 mL), were added HOBt (2.15 g, 15.94 mmol), EDCI (3.06 g, 15.94 mmol), and NMM (8.76 mL, 79.72 mmol). The mixture was stirred at r.t. overnight before EtOAc (150 mL) and water (100 mL) were added. The aqueous phase was extracted with EtOAc (2 × 100 mL). The combined organic phases were dried over anhydrous Na_2SO_4 and concentrated under reduced pressure. The residue was purified by silica gel flash column chromatography with EtOAc/PE (10−35%) to afford **6** as a yellow solid (3.7 g, 58.3% yield). ^1H NMR (400 MHz, $CDCl_3$) δ 11.12 (s, 1H), 7.22 (d, J = 1.8 Hz, 1H), 7.18 (d, J = 1.8 Hz, 1H), 7.12 (t, J = 5.6 Hz, 1H), 5.95 (s, 1H), 4.52 (d, J = 5.9 Hz, 2H), 3.95 (d, J = 11.4 Hz, 2H), 3.35−3.27 (m, 2H), 3.02 (q, J = 6.9 Hz, 2H), 2.93 (m, 1H), 2.39 (s, 3H), 2.24 (d, J = 2.3 Hz, 6H), 1.66 (m, 4H), 0.85 (t, J = 7.0 Hz, 3H).

*3′-(((4,6-Dimethyl-2-oxo-1,2-dihydropyridin-3-yl)methyl)-carbamoyl)-5′-(ethyl(tetrahydro-2H-pyran-4-yl)amino)-4′-methyl-[1,1′-biphenyl]-4-carboxylic Acid (**7**).*[40] To a solution of **6** (1 g, 2.10 mmol) in DMF (20 mL) were added 4-methoxycarbonylphenylboronic acid (453 mg, 2.52 mmol), K_2CO_3 (1.16 g, 8.40 mmol), and $Pd(PPh_3)_4$ (121 mg, 104.95 μmol). The solution was purged and refilled with argon three times. Then, the solution was stirred at 90 °C for 9 h before EtOAc (70 mL) and water (30 mL) were added at r.t. The aqueous phase was extracted with EtOAc (2 × 70 mL). The combined organic phases were dried over Na_2SO_4, filtered, and concentrated under reduced pressure. The residue was purified by flash column chromatography with $MeOH/CH_2Cl_2$ (0−10%) to afford the coupled product as a yellow solid (0.82 g, 73.5% yield). The obtained product was hydrolyzed under NaOH in EtOH at 60 °C to give the final acid **7**. ^1H NMR (500 MHz, $CDCl_3$) δ 12.96 (s, 1H), 8.17 (d, J = 8.2 Hz, 2H), 7.69 (m, 3H), 7.51 (s, 1H), 7.41 (s, 1H), 6.12 (s, 1H), 4.51 (d, J = 5.8 Hz, 2H), 3.96 (d, J = 11.3 Hz, 2H), 3.33 (t, J = 11.0 Hz, 2H), 3.15 (s, 2H), 3.06 (s, 1H), 2.50 (d, J = 15.6 Hz, 6H), 2.37 (s, 3H), 1.72 (m, 4H), 0.92 (t, J = 6.4 Hz, 3H).

*tert-Butyl((S)-1-((2S,4R)-4-hydroxy-2-((4-(4-methylthiazol-5-yl)-benzyl)carbamoyl)pyrrolidin-1-yl)-3,3-dimethyl-1-oxobutan-2-yl)-carbamate (**15**).*[31,43] To a solution of (4-bromophenyl)methanamine **8** (6.79 mL, 53.75 mmol) in MeOH (80 mL) were added Boc_2O (18.52 mL, 80.62 mmol) and NaOH (107.5 mmol, 1 M) at 0 °C. The reaction mixture was warmed to r.t. and stirred for 5 h. MeOH was removed under reduced pressure, and the residue was acidified by adding aq. HCl until pH = 5. The aqueous solution was extracted with CH_2Cl_2 (3 × 150 mL). The combined organic phases were washed with brine, dried over anhydrous Na_2SO_4, and filtered. The concentration under reduced pressure gave a colorless liquid (14.4 g, 93.6% yield), which was used in the next step without further purification.

To a solution of the above-obtained liquid (14.4 g, 50.42 mmol) in DMA (50 mL) under argon were added $Pd(AcO)_2$ (226.45 mg, 1.01 mmol), potassium acetate (9.9 g, 100.86 mmol), and 4-methylthiazole **9** (4.59 mL, 50.43 mmol). The reaction mixture was stirred at 150 °C for 10 h. Then, CH_2Cl_2 (150 mL) and water (100 mL) were added. The aqueous phase was extracted with CH_2Cl_2 (2 × 150 mL). The combined organic phases were dried over anhydrous Na_2SO_4, filtered, concentrated under reduced pressure to give **10** as a yellow liquid (14.35 g, 93.7% yield), which was used in the next step without further purification. After the removal of the Boc group in **10** (6.5 g. 21.35 mmol) under acidic conditions, a free amine residue (5.14 g, 20.77 mmol) was obtained. To a stirred solution of **12** (5.92 g, 25.62 mmol) and DIPEA (10.59 mL, 64.05 mmol) in anhydrous THF (75 mL) at 0 °C were added the above-obtained amine (5.14 g, 20.77 mmol) and HATU (9.74, 25.62 mmol). The resulting mixture was warmed to r.t. and stirred for 2 h. After THF was removed under reduced pressure, CH_2Cl_2 (120 mL) and water (80 mL) were added. The aqueous phase was extracted with CH_2Cl_2 (2 × 100 mL). The combined organic phases were dried over anhydrous Na_2SO_4, filtered, and concentrated under reduced pressure to give **13** as a yellow liquid (8.67 g, 82.5% yield), which was used in the next step without further purification. After the removal of the Boc group in **13** (5 g, 11.98 mmol) under acidic conditions, the obtained free amine residue was added to the stirred solution of *N*-Boc-L-*tert*-Leucine **14** (2.76 g, 11.93 mmol), DIPEA (5.91 mL, 35.78 mmol), and HATU (6.8 g, 17.89 mmol) in DMF (45 mL). The reaction mixture was stirred at r.t. for 5 h. CH_2Cl_2 (120 mL) and water (60 mL) were added, and the aqueous phase was extracted with CH_2Cl_2 (2 × 100 mL). The combined organic phases were dried over anhydrous Na_2SO_4, filtered, and concentrated under reduced pressure. The residue was purified by column chromatography on silica gel with $MeOH/CH_2Cl_2$ (0−10%) to give **15** as a yellow solid (4.5 g, 70.8% yield). ^1H NMR (400 MHz, $CDCl_3$) δ 8.68 (s, 1H), 7.47 (m, 1H), 7.33 (m, 4H), 5.20 (d, J = 9.0 Hz, 1H), 4.74 (m, 1H), 4.53(m, 2H), 4.30 (dd, J = 15.0, 5.1 Hz, 1H), 4.17 (d, J = 9.1 Hz, 1H), 4.02 (d, J = 11.3 Hz, 1H), 3.60 (dd, J = 11.3, 3.4 Hz, 1H), 2.50 (s, 3H), 2.50 (m, 1H), 2.10 (m, 1H), 1.40 (s, 9H), 0.91 (s, 9H).

*(2S,4R)-1-((S)-2-Acetamido-3,3-dimethylbutanoyl)-4-hydroxy-N-(4-(4-methylthiazol-5-yl)benzyl)pyrrolidine-2-carboxamide (**VH032**).*[31,43] Removal of the Boc group in **15** (50 mg, 94.22 mmol) under acidic conditions afforded amine compound **16**. To a solution of **16** (40 mg, 94.22 μmol) in CH_2Cl_2 was added DIPEA (46.06 μL,

https://doi.org/10.1021/acs.jmedchem.1c00460
J. Med. Chem. 2021, 64, 10167−10184

278.70 μmol) at 0 °C. After the mixture was stirred for 0.5 h at r.t., acetic anhydride (13.17 μL, 139.35 μmol) was added. The mixture was continued to stir at r.t. for 2 h. CH_2Cl_2 (10 mL) and water (5 mL) were added, and the mixture was extracted with CH_2Cl_2 (2 × 10 mL). The combined organic phases were dried over anhydrous Na_2SO_4, filtered, and concentrated under reduced pressure. The residue was purified by column chromatography on silica gel with MeOH/CH_2Cl_2 (0−10%) to give **VH032** as a yellow solid (32 mg, 67.7% yield). ^{1}H NMR (400 MHz, $CDCl_3$) δ 8.68 (s, 1H), 7.36 (q, *J* = 8.3 Hz, 4H), 6.32 (d, *J* = 8.6 Hz, 1H), 4.70 (t, *J* = 8.0 Hz, 1H), 4.65−4.47 (m, 3H), 4.33 (dd, *J* = 15.0, 5.1 Hz, 1H), 4.10 (d, *J* = 11.5 Hz, 1H), 3.61 (dd, *J* = 11.4, 3.3 Hz, 1H), 2.51 (s, 3H), 2.51 (m, 1H), 2.14 (dd, *J* = 13.6, 8.4 Hz, 1H), 1.98 (s, 3H), 0.93 (s, 9H).

*2-(2,6-Dioxopiperidin-3-yl)-4-fluoroisoindoline-1,3-dione (**32**).*[41] To a suspension of 4-fluoroisobenzofuran-1,3-dione **29** (1 g, 6.02 mmol) and 3-aminopiperidine-2,6-dione hydrochloride **31** (0.99 g, 6.02 mmol) in AcOH (20 mL) was added sodium acetate (0.59 g, 7.22 mmol). The reaction mixture was heated to 120 °C for 12 h. After cooling to r.t., AcOH was removed under reduced pressure. The residue was purified by flash column chromatography with MeOH/CH_2Cl_2 (0−10%) to give **32** as a white solid (1.33 g, 79.7% yield). ^{1}H NMR (400 MHz, d_6-DMSO) δ 11.14 (s, 1H), 7.98−7.91 (m, 1H), 7.79 (d, *J* = 7.3 Hz, 1H), 7.74 (t, *J* = 8.9 Hz, 1H), 5.16 (dd, *J* = 12.9, 5.4 Hz, 1H), 2.89 (ddd, *J* = 17.2, 14.0, 5.5 Hz, 1H), 2.68−2.52 (m, 2H), 2.06 (ddd, *J* = 10.7, 5.5, 3.1 Hz, 1H).

*2-(2,6-Dioxopiperidin-3-yl)-4-hydroxyisoindoline-1,3-dione (**33**).*[42] 3-Hydroxyphthalic anhydride **30** (3 g, 18.28 mmol) and 3-aminopiperidine-2,6-dione hydrochloride **31** (2.99 g, 18.28 mmol) were dissolved in pyridine (80 mL) and heated to 110 °C. After 14 h, the mixture was cooled to r.t. and concentrated under reduced pressure. The residue was purified by flash column chromatography with MeOH/CH_2Cl_2 (0−10%) to give **33** as a tan solid (4.02 g, 80.2% yield). ^{1}H NMR (500 MHz, d_6-DMSO) δ 11.18 (s, 1H), 11.09 (s, 1H), 7.65 (t, *J* = 7.7 Hz, 1H), 7.32 (d, *J* = 7.0 Hz, 1H), 7.25 (d, *J* = 8.4 Hz, 1H), 5.07 (dd, *J* = 12.8, 5.2 Hz, 1H), 2.93−2.83 (m, 1H), 2.55 (dd, *J* = 27.8, 11.8 Hz, 2H), 2.01 (dd, *J* = 13.6, 7.8 Hz, 1H).

*(2S,4R)-1-((S)-2-(2-(3-((3′-(((4,6-Dimethyl-2-oxo-1,2-dihydropyridin-3-yl)methyl)carbamoyl)-5′-(ethyl(tetrahydro-2H-pyran-4-yl)amino)-4′-methyl-[1,1′-biphenyl]-4-yl)oxy)propoxy)acetamido)-3,3-dimethylbutanoyl)-4-hydroxy-N-(4-(4-methylthiazol-5-yl)benzyl)pyrrolidine-2-carboxamide (**V2**, **YM281**).* To a solution of 1,3-propanediol **17b** (2 g, 26.28 mmol) in THF (10 mL) was added NaH (60%, 525.61 mg, 131.14 mmol) at 0 °C. The reaction mixture was stirred for 1 h before BnBr (1.04 mL, 8.76 mmol) was added at 0 °C. The reaction mixture was gradually warmed to r.t., stirred overnight, and quenched with saturated aq. NH_4Cl (30 mL). The mixture was extracted with EtOAc (3 × 80 mL). The combined organic phases were dried over Na_2SO_4, filtered, and concentrated under reduced pressure. The residue was purified by flash column chromatography with EtOAc/PE (10−50%) to afford 3-(benzyloxy)-propan-1-ol as a colorless oil (0.82 g, 56.3% yield).

A mixture of 3-(benzyloxy)propan-1-ol (0.81 g, 4.87 mmol), *tert*-butyl bromoacetate (2.84 mL, 19.5 mmol), aqueous sodium hydroxide (35%, 20 mL), and TBACl (1.38 mL, 4.87 mmol) in CH_2Cl_2 (20 mL) was stirred vigorously at r.t. overnight. The reaction mixture was poured into water (15 mL) and then was extracted with CH_2Cl_2 (3 × 20 mL). The combined organic phases were washed with water (15 mL × 2) and brine (2 × 15 mL), dried over anhydrous Na_2SO_4, and concentrated under reduced pressure. The residue was purified by flash column chromatography with EtOAc/PE (0−20%) to afford **18b** as a colorless oil (1.2 g, 87.8% yield).

A mixture of **18b** (670 mg, 2.39 mmol) and palladium on carbon (10%, 70 mg) in ethanol (8 mL) was stirred at r.t. overnight under a hydrogen atmosphere. The mixture was filtered and washed with EtOAc (3 × 30 mL). The combined filtrate was concentrated under reduced pressure to afford a hydroxyl product as a colorless oil, which was used in the next step without further purification. The hydroxyl product (454 mg, 2.39 mmol) was dissolved in CH_2Cl_2 (5 mL), followed by the addition of 4-toluenesulfonyl chloride (901 mg, 4.73 mmol), TEA (658 μL, 4.73 mmol), and DMAP (145 mg, 1.18 mmol). The reaction mixture was stirred at r.t. for 3 h before it was diluted with CH_2Cl_2 (100 mL). The organic phase was washed with water (3 × 10 mL), dried over Na_2SO_4, and concentrated under reduced pressure. The residue was purified by flash column chromatography with EtOAc/PE (20−50%) to afford **19b** as a colorless oil (450 mg, 54.8% yield).

To a solution of **19b** (150 mg, 435 μmol) in DMF (2 mL) were added 4-hydroxyphenylboronic acid pinacol ester (144 mg, 653 μmol) and K_2CO_3 (120 mg, 871 μmol). The reaction mixture was stirred at 70 °C for 5 h and then cooled to r.t. before EtOAc (30 mL) and water (10 mL) were added. The mixture was extracted with EtOAc (2 × 30 mL). The combined organic phases were dried over Na_2SO_4, filtered, and concentrated under reduced pressure. The residue was purified by flash column chromatography with EtOAc/PE (20−50%) to afford **20b** as a colorless solid (145 mg, 84.9% yield).

To a solution of **6** (121.4 mg, 254.9 μmol) in DMF (2 mL) were added **20b** (100 mg, 254.91 μmol), K_2CO_3 (108.2 mg, 509 μmol), and $Pd(PPh_3)_4$ (14.7 mg, 12.75 μmol). The mixture was purged and refilled with argon three times. The mixture was stirred at 90 °C for 9 h before EtOAc (30 mL) and water (10 mL) were added at r.t. The aqueous phase was extracted with EtOAc (2 × 30 mL). The combined organic phases were dried over Na_2SO_4, filtered, and concentrated under reduced pressure. The residue was purified by flash column chromatography with MeOH/CH_2Cl_2 (0−10%) to afford the coupled product as a yellow solid (120 mg, 71.1% yield).

Then, the obtained product (120 mg, 181.32 μmol) was dissolved in CH_2Cl_2 (1 mL), and TFA (135 μL, 1.81 mmol) was added before the mixture was stirred at r.t. for 3 h. The concentration of the solvent provided acid **21b**, which was used for the following steps without further purification. To a stirred solution of **21b** in DMF (2 mL), amine **16** (92.98 mg, 215.94 mmol), DIPEA (178.45 μL, 1.08 mmol), and HATU (68.42 mg 179.95 μmol) were added sequentially. The resulting mixture was stirred at r.t. for 10 h, and then brine (5 mL) was added and extracted with EtOAc (3 × 15 mL). The combined organic phases were washed with brine, dried over anhydrous Na_2SO_4, filtered, and concentrated under reduced pressure. The residue was purified by flash column chromatography with MeOH/CH_2Cl_2 (0−10%) to give **V2** (**YM281**) as a white powder (118 mg, 64.4% yield). ^{1}H NMR (500 MHz, d_6-DMSO) δ 11.47 (s, 1H), 8.95 (s, 1H), 8.60 (s, 1H), 8.18 (s, 1H), 7.51 (d, *J* = 7.8 Hz, 2H), 7.44 (d, *J* = 8.8 Hz, 1H), 7.38 (m, 4H), 7.32 (s, 1H), 7.16 (s, 1H), 7.01 (d, *J* = 7.4 Hz, 2H), 5.85 (s, 1H), 5.17 (s, 1H), 4.57 (d, *J* = 9.3 Hz, 1H), 4.46 (t, *J* = 8.1 Hz, 1H), 4.38 (d, *J* = 15.9 Hz, 2H), 4.33−4.21 (m, 3H), 4.10 (s, 2H), 3.97 (s, 2H), 3.81 (d, *J* = 9.9 Hz, 2H), 3.71−3.58 (m, 4H), 3.23 (t, *J* = 11.2 Hz, 2H), 3.06 (d, *J* = 6.3 Hz, 2H), 2.99 (s, 1H), 2.41 (s, 3H), 2.23 (s, 3H), 2.20 (s, 3H), 2.10 (s, 3H), 2.07−1.98 (m, 3H), 1.91 (s, 1H), 1.64 (d, *J* = 11.2 Hz, 2H), 1.50 (d, *J* = 10.6 Hz, 2H), 0.94 (s, 9H), 0.81 (t, *J* = 5.9 Hz, 3H). ^{13}C NMR (125 MHz, d_6-DMSO) δ 171.7, 169.2, 169.1, 168.4, 163.0, 158.1, 151.4, 149.5, 148.8, 147.7, 142.7, 139.6, 139.4, 136.9, 132.3, 131.9, 131.1, 129.7, 128.9, 128.7, 128.2, 127.7, 127.5, 122.5, 121.6, 120.5, 114.9, 107.4, 69.5, 68.9, 67.7, 66.3, 64.6, 58.8, 57.9, 56.6, 55.7, 41.7, 41.2, 37.9, 35.8, 34.9, 30.3, 29.0, 26.2, 19.0, 18.2, 15.9, 14.5, 12.7. HRMS (ESI, *m*/*z*) calcd for $C_{56}H_{72}N_7O_9S$ $[M + H]^+$: 1018.5107, found: 1018.5121. Purity: 98.1%.

*(2S,4R)-1-((S)-2-(2-(2-((3′-(((4,6-Dimethyl-2-oxo-1,2-dihydropyridin-3-yl)methyl)carbamoyl)-5′-(ethyl(tetrahydro-2H-pyran-4-yl)amino)-4′-methyl-[1,1′-biphenyl]-4-yl)oxy)ethoxy)acetamido)-3,3-dimethylbutanoyl)-4-hydroxy-N-(4-(4-methylthiazol-5-yl)benzyl)pyrrolidine-2-carboxamide (**V1**).* **V1** was prepared following the procedure for the synthesis of compound **V2** (**YM281**). ^{1}H NMR (400 MHz, d_6-DMSO) δ 11.47 (s, 1H), 8.92 (s, 1H), 8.63 (t, *J* = 5.9 Hz, 1H), 8.17 (t, *J* = 4.8 Hz, 1H), 7.53−7.46 (m, 3H), 7.42 (d, *J* = 8.3 Hz, 2H), 7.36 (d, *J* = 8.2 Hz, 2H), 7.29 (s, 1H), 7.15 (s, 1H), 7.09 (d, *J* = 8.7 Hz, 2H), 5.85 (s, 1H), 5.18 (d, *J* = 3.4 Hz, 1H), 4.61 (d, *J* = 9.6 Hz, 1H), 4.51−4.34 (m, 3H), 4.30 (d, *J* = 4.8 Hz, 2H), 4.26 (d, *J* = 5.5 Hz, 1H), 4.24−4.12 (m, 2H), 4.06 (s, 2H), 3.86 (t, *J* = 4.3 Hz, 2H), 3.80 (d, *J* = 11.7 Hz, 2H), 3.69 (dd, *J* = 10.5, 3.7 Hz, 1H), 3.62 (d, *J* = 10.8 Hz, 1H), 3.22 (t, *J* = 11.0 Hz, 2H), 3.08−3.01 (m, 2H), 3.01−2.92 (m, 1H), 2.38 (s, 3H), 2.22 (s, 3H), 2.21 (s, 3H), 2.10 (s,

https://doi.org/10.1021/acs.jmedchem.1c00460
J. Med. Chem. 2021, 64, 10167−10184

3H), 2.09−2.02 (m, 1H), 1.96−1.88 (m, 1H), 1.63 (d, J = 11.4 Hz, 2H), 1.55−1.45 (m, 2H), 0.94 (s, 9H), 0.79 (t, J = 7.0 Hz, 3H). ^{13}C NMR (101 MHz, d_6-DMSO) δ 171.8, 169.1, 168.4, 163.0, 158.0, 151.3, 149.5, 148.8, 147.6, 142.7, 139.5, 139.4, 136.8, 132.4, 131.9, 131.1, 129.6, 128.8, 128.6, 128.1, 127.6, 127.4, 122.5, 121.6, 120.5, 115.0, 107.4, 69.6, 69.5, 68.9, 70.0, 66.3, 58.8, 57.8, 56.6, 55.7, 41.7, 41.2, 37.9, 35.8, 34.9, 30.3, 26.2, 18.9, 18.9, 18.2, 15.9, 14.5, 12.7. HRMS (ESI, m/z) calcd for $C_{55}H_{70}N_7O_9S$ $[M + H]^+$: 1004.4805, found: 1004.4805. Purity: 98.1%.

*(2S,4R)-1-((S)-2-(2-(2-(2-((3′-(((4,6-Dimethyl-2-oxo-1,2-dihydropyridin-3-yl)methyl)carbamoyl)-5′-(ethyl(tetrahydro-2H-pyran-4-yl)amino)-4′-methyl-[1,1′-biphenyl]-4-yl)oxy)ethoxy)ethoxy)-acetamido)-3,3-dimethylbutanoyl)-4-hydroxy-N-(4-(4-methylthiazol-5-yl)benzyl)pyrrolidine-2-carboxamide (**V3**, **YM181**).* **V3** was prepared following the procedure for the synthesis of compound **V2** (**YM281**). ^{1}H NMR (500 MHz, d_6-DMSO) δ 11.46 (s, 1H), 8.95 (s, 1H), 8.59 (t, J = 5.6 Hz, 1H), 8.17 (s, 1H), 7.51 (d, J = 8.1 Hz, 2H), 7.45 (d, J = 9.5 Hz, 1H), 7.42−7.36 (m, 4H), 7.33 (s, 1H), 7.17 (s, 1H), 6.98 (d, J = 8.0 Hz, 2H), 5.85 (s, 1H), 5.16 (s, 1H), 4.57 (d, J = 9.5 Hz, 1H), 4.45 (t, J = 8.0 Hz, 1H), 4.38 (dd, J = 16.4, 6.1 Hz, 2H), 4.29 (d, J = 4.2 Hz, 2H), 4.25 (dd, J = 16.0, 5.3 Hz, 1H), 4.13 (s, 2H), 3.97 (d, J = 16.9 Hz, 2H), 3.80 (t, J = 14.1 Hz, 4H), 3.70−3.59 (m, 4H), 3.23 (t, J = 11.4 Hz, 2H), 3.06 (d, J = 6.6 Hz, 2H), 3.01 (d, J = 10.2 Hz, 1H), 2.42 (s, 3H), 2.23 (s, 3H), 2.20 (s, 3H), 2.10 (s, 3H), 2.05 (d, J = 7.3 Hz, 1H), 1.98 (dd, J = 17.1, 10.8 Hz, 1H), 1.91 (dd, J = 14.8, 6.5 Hz, 1H), 1.65 (d, J = 11.4 Hz, 2H), 1.57−1.44 (m, 2H), 0.94 (s, 9H), 0.82 (t, J = 6.7 Hz, 3H). ^{13}C NMR (101 MHz, d_6-DMSO) δ 171.8, 169.2, 168.7, 163.1, 158.1, 151.4, 149.6, 147.8, 142.8, 139.5, 139.4, 136.9, 132.3, 132.0, 131.2, 129.7, 128.7, 127.7, 127.5, 122.6, 121.6, 120.5, 114.9, 107.5, 70.5, 69.8, 69.7, 69.1, 68.9, 67.2, 66.4, 58.8, 57.9, 56.6, 55.8, 41.7, 37.9, 35.8, 34.9, 31.3, 30.4, 29.0, 26.2, 25.2, 22.1, 21.4, 19.0, 18.2, 15.9, 14.5, 14.0, 12.7. HRMS (ESI, m/z) calcd for $C_{57}H_{74}N_7O_{10}S$ $[M + H]^+$: 1048.5212, found: 1048.5216. Purity: 96.3%.

*N^3-((4,6-Dimethyl-2-oxo-1,2-dihydropyridin-3-yl)methyl)-5-(ethyl(tetrahydro-2H-pyran-4-yl)amino)-$N^{4'}$-(2-(2-(2-(((S)-1-((2S,4R)-4-hydroxy-2-((4-(4-methylthiazol-5-yl)benzyl)carbamoyl)-pyrrolidin-1-yl)-3,3-dimethyl-1-oxobutan-2-yl)amino)-2-oxoethoxy)ethoxy)ethyl)-4-methyl-[1,1′-biphenyl]-3,4′-dicarboxamide (**V4**).* **V4** was prepared following the procedure for the synthesis of compound **V2** (**YM281**). ^{1}H NMR (400 MHz, d_6-DMSO) δ 11.44 (s, 1H), 8.95 (s, 1H), 8.60−8.50 (m, 2H), 8.20 (t, J = 5.0 Hz, 1H), 7.91 (d, J = 8.4 Hz, 2H), 7.70 (d, J = 8.4 Hz, 2H), 7.44 (d, J = 9.9 Hz, 2H), 7.38 (brs, 4H), 7.29 (s, 1H), 5.86 (s, 1H), 5.16 (d, J = 3.5 Hz, 1H), 4.57 (d, J = 9.6 Hz, 1H), 4.47 (d, J = 8.1 Hz, 1H), 4.35 (d, J = 6.0 Hz, 2H), 4.30 (d, J = 4.8 Hz, 2H), 4.25 (dd, J = 15.8, 5.7 Hz, 1H), 3.97 (s, 2H), 3.82 (d, J = 10.3 Hz, 2H), 3.70−3.55 (m, 8H), 3.46 (d, J = 5.8 Hz, 2H), 3.25 (t, J = 11.2 Hz, 2H), 3.15−2.97 (m, 3H), 2.43 (s, 3H), 2.25 (s, 3H), 2.21 (s, 3H), 2.10 (s, 3H), 2.06 (s, 1H), 1.90 (s, 1H), 1.66 (d, J = 11.7 Hz, 2H), 1.52 (d, J = 8.8 Hz, 2H), 0.93 (s, 9H), 0.83 (t, J = 7.0 Hz, 3H). ^{13}C NMR (101 MHz, d_6-DMSO) δ 171.7, 169.2, 168.9, 168.6, 165.9, 163.0, 151.4, 149.5, 149.0, 147.7, 142.3, 139.7, 139.4, 136.2, 133.1, 131.1, 129.7, 128.7, 127.8, 127.4, 126.4, 123.0, 121.0, 99.5, 70.4, 69.6, 69.4, 69.0, 68.8, 66.3, 58.7, 57.9, 56.6, 55.7, 41.7, 41.2, 37.9, 35.7, 34.9, 30.3, 26.2, 18.9, 18.2, 15.9, 14.6, 12.8. HRMS (ESI, m/z) calcd for $C_{58}H_{73}N_8O_{10}S$ $[M - H]^-$: 1073.5176, found: 1073.5195. Purity: 95.8%.

*(2S,4R)-1-((S)-2-(tert-Butyl)-14-((3′-(((4,6-dimethyl-2-oxo-1,2-dihydropyridin-3-yl)methyl)carbamoyl)-5′-(ethyl(tetrahydro-2H-pyran-4-yl)amino)-4′-methyl-[1,1′-biphenyl]-4-yl)oxy)-4-oxo-6,9,12-trioxa-3-azatetradecanoyl)-4-hydroxy-N-(4-(4-methylthiazol-5-yl)benzyl)pyrrolidine-2-carboxamide (**V5**).* **V5** was prepared following the procedure for the synthesis of compound **V2** (**YM281**). ^{1}H NMR (400 MHz, d_6-DMSO) δ 11.47 (s, 1H), 8.97 (d, J = 3.9 Hz, 1H), 8.60 (t, J = 5.9 Hz, 1H), 8.17 (t, J = 4.8 Hz, 1H), 7.53 (d, J = 8.6 Hz, 2H), 7.43 (d, J = 4.6 Hz, 1H), 7.41 (s, 1H), 7.38 (d, J = 9.1 Hz, 4H), 7.35 (s, 1H), 7.18 (s, 1H), 6.99 (d, J = 8.7 Hz, 2H), 5.85 (s, 1H), 5.17 (s, 1H), 4.57 (d, J = 9.6 Hz, 1H), 4.50−4.39 (m, 1H), 4.37 (d, J = 6.1 Hz, 2H), 4.33−4.20 (m, 3H), 4.13−4.06 (m, 2H), 3.97 (s, 2H), 3.82 (d, J = 10.2 Hz, 3H), 3.76−3.71 (m, 2H), 3.60 (m, 6H), 3.24 (t, J = 11.2 Hz, 2H), 3.17 (s, 2H), 3.11-3.03 (m, 2H), 3.01 (s, 1H), 2.43 (s, 3H), 2.23 (s, 3H), 2.21 (s, 3H), 2.10 (s, 3H), 2.08−2.03 (m, 1H), 1.95−1.86 (m, 1H), 1.65 (d, J = 10.9 Hz, 2H), 1.57−1.45 (m, 2H), 0.94 (s, 9H), 0.82 (t, J = 6.9 Hz, 3H). ^{13}C NMR (101 MHz, d_6-DMSO) δ 171.8, 169.1, 168.6, 163.0, 158.0, 151.4, 149.5, 148.8, 147.7, 14.7, 139.5, 139.4, 136.9, 132.3, 132.0, 131.1, 129.7, 128.7, 127.6, 127.5, 122.5, 121.6, 120.5, 114.9, 107.4, 70.5, 69.9, 69.9, 69.6, 68.9, 68.9, 67.2, 66.3, 58.8, 57.9, 56.6, 55.7, 48.6, 41.7, 41.2, 37.9, 35.7, 34.9, 30.3, 26.2, 18.9, 18.2, 15.9, 14.5, 12.7 HRMS (ESI, m/z) calcd for $C_{59}H_{76}N_7O_{11}S$ $[M - H]^-$: 1090.5329, found: 1090.5319. Purity: 98.4%.

*N^3-((4,6-Dimethyl-2-oxo-1,2-dihydropyridin-3-yl)methyl)-5-(ethyl(tetrahydro-2H-pyran-4-yl)amino)-$N^{4'}$-((S)-14-((2S,4R)-4-hydroxy-2-((4-(4-methylthiazol-5-yl)benzyl)carbamoyl)pyrrolidine-1-carbonyl)-15,15-dimethyl-12-oxo-3,6,9-trioxa-13-azahexadecyl)-4-methyl-[1,1′-biphenyl]-3,4′-dicarboxamide (**V6**).* **V6** was prepared following the procedure for the synthesis of compound **V2** (YM281). ^{1}H NMR (400 MHz, d_6-DMSO) δ 11.45 (s, 1H), 8.97 (s, 1H), 8.55 (t, J = 5.7 Hz, 2H), 8.21 (t, J = 4.9 Hz, 2H), 7.91 (d, J = 8.4 Hz, 2H), 7.89 (d, J = 9.5 Hz, 1H), 7.72 (d, J = 8.3 Hz, 2H), 7.46 (s, 1H), 7.40 (q, J = 8.3 Hz, 4H), 7.30 (s, 1H), 5.87 (s, 1H), 5.14 (d, J = 3.5 Hz, 1H), 4.55 (d, J = 9.4 Hz, 1H), 4.42 (m, 2H), 4.35 (s, 1H), 4.30 (d, J = 4.9 Hz, 2H), 4.22 (dd, J = 15.8, 5.4 Hz, 2H), 4.01−3.95 (m, 1H), 3.83 (d, J = 10.8 Hz, 2H), 3.70−3.41 (m, 15H), 3.29−3.20 (m, 2H), 3.15−2.99 (m, 3H), 2.44 (s, 3H), 2.26 (s, 3H), 2.22 (s, 3H), 2.11 (s, 3H), 2.03 (m, 1H), 1.97−1.86 (m, 1H), 1.67 (d, J = 11.3 Hz, 2H), 1.54−1.48 (m, 2H), 0.93 (s, 9H), 0.83 (t, J = 7.0 Hz, 3H). ^{13}C NMR (101 MHz, d_6-DMSO) δ 171.9, 170.0, 169.6, 169.0, 166.0, 163.0, 151.4, 149.6, 149.0, 147.7, 142.8, 142.8, 142.3, 139.7, 139.5, 136.2, 133.5, 133.1, 131.2, 129.7, 128.6, 127.8, 127.4, 126.4, 124.0, 123.1, 121.6, 121.0, 107.4, 69.7, 69.6, 69.5, 68.9, 66.9, 66.3, 58.7, 57.9, 56.3, 41.7, 41.3, 41.2, 37.9, 35.7, 35.3, 34.9, 30.3, 26.3, 19.0, 18.6, 18.2, 15.9, 14.6, 12.8. HRMS (ESI, m/z) calcd for $C_{61}H_{79}N_8O_{11}S$ $[M - H]^-$: 1131.5594, found: 1131.5584. Purity: 99.1%.

*N^3-((4,6-Dimethyl-2-oxo-1,2-dihydropyridin-3-yl)methyl)-5-(ethyl(tetrahydro-2H-pyran-4-yl)amino)-$N^{4'}$-((S)-17-((2S,4R)-4-hydroxy-2-((4-(4-methylthiazol-5-yl) benzyl) carbamoyl) pyrrolidine-1-carbonyl)-18,18-dimethyl-15-oxo-3,6,9,12-tetraoxa-16-azanonadecyl)-4-methyl-[1,1′-biphenyl]-3,4′-dicarboxamide (**V7**).* **V7** was prepared following the procedure for the synthesis of compound **V2** (**YM281**). ^{1}H NMR (400 MHz, d_6-DMSO) δ 11.47 (s, 1H), 8.98 (s, 1H), 8.58 (s, 2H), 8.23 (s, 1H), 7.93 (d, J = 8.2 Hz, 3H), 7.72 (d, J = 8.0 Hz, 2H), 7.46 (s, 1H), 7.39 (dd, J = 16.2, 7.9 Hz, 4H), 7.29 (s, 1H), 5.86 (s, 1H), 5.15 (s, 1H), 4.55 (d, J = 9.3 Hz, 1H), 4.42 (d, J = 4.8 Hz, 2H), 4.35 (s, 1H), 4.30 (d, J = 4.0 Hz, 2H), 4.26−4.16 (m, 1H), 4.08−4.01 (m, 1H), 3.98 (t, J = 6.5 Hz, 1H), 3.83 (d, J = 10.2 Hz, 2H), 3.70−3.59 (m, 4H), 3.55-3.48 (m, 8H), 3.45 (d, J = 4.9 Hz, 2H), 3.25 (t, J = 11.2 Hz, 3H), 3.17−2.96 (m, 3H), 2.44 (s, 3H), 2.25 (s, 3H), 2.21 (s, 3H), 2.10 (s, 3H), 2.07−2.00 (m, 1H), 1.99 (s, 1H), 1.90 (s, 1H), 1.66 (d, J = 10.9 Hz, 2H), 1.52 (d, J = 7.4 Hz, 4H), 1.31 (d, J = 6.9 Hz, 2H), 0.93 (s, 9H), 0.83 (t, J = 7.0 Hz, 3H). ^{13}C NMR (101 MHz, d_6-DMSO) δ 172.0, 170.1, 169.6, 169.3, 169.0, 166.0, 163.1, 151.5, 149.7, 149.1, 147.7, 142.8, 142.4, 139.8, 139.5, 136.3, 133.5, 133.1, 131.2, 129.7, 128.7, 127.9, 127.5, 126.4, 123.1, 121.6, 121.1, 107.5, 72.9, 69.8, 69.8, 69.7, 69.7, 69.5, 68.9, 68.9, 66.9, 66.4, 63.8, 58.8, 57.9, 56.4, 48.6, 43.1, 41.7, 41.3, 38.0, 35.7, 35.4, 35.0, 30.4, 30.1, 30.0, 26.4, 19.0, 18.6, 18.2, 15.9, 14.7, 13.6, 12.8. HRMS (ESI, m/z) calcd for $C_{63}H_{83}N_8O_{12}S$ $[M - H]^-$: 1175.5857, found: 1175.5874. Purity: 97.7%.

*(2R,4S)-1-((S)-2-(2-(2-(3-((3′-(((4,6-Dimethyl-2-oxo-1,2-dihydropyridin-3-yl)methyl)carbamoyl)-5′-(ethyl(tetrahydro-2H-pyran-4-yl)-amino)-4′-methyl-[1,1′-biphenyl]-4-yl)oxy)propoxy)acetamido)-3,3-dimethylbutanoyl)-4-hydroxy-N-(4-(4-methylthiazol-5-yl)-benzyl)pyrrolidine-2-carboxamide (**YM620**).* **YM620** was prepared from **21b** and **41** following the procedure for the synthesis of compound **V2** (**YM281**). ^{1}H NMR (400 MHz, d_6-DMSO) δ 11.46 (s, 1H), 8.96 (s, 1H), 8.35 (t, J = 5.9 Hz, 1H), 8.17 (t, J = 4.9 Hz, 1H), 7.52 (d, J = 8.6 Hz, 2H), 7.45−7.37 (m, 4H), 7.32 (t, J = 6.3 Hz, 3H), 7.18 (s, 1H), 6.97 (d, J = 8.7 Hz, 2H), 5.86 (s, 1H), 5.14 (d, J = 3.5 Hz, 1H), 4.54 (d, J = 9.0 Hz, 1H), 4.44−4.33 (m, 3H), 4.30 (d, J = 4.5 Hz, 3H), 4.25 (d, J = 5.8 Hz, 1H), 4.04 (t, J = 6.3 Hz, 2H), 3.82 (d, J = 10.5 Hz, 2H), 3.75 (dd, J = 10.3, 4.7 Hz, 1H), 3.59 (d, J = 6.5

https://doi.org/10.1021/acs.jmedchem.1c00460
J. Med. Chem. 2021, 64, 10167−10184

Hz, 3H), 3.24 (t, J = 11.1 Hz, 3H), 3.12−3.04 (m, 2H), 3.01 (s, 1H), 2.43 (s, 3H), 2.24 (s, 3H), 2.21 (s, 3H), 2.11 (s, 3H), 2.06 (dd, J = 8.2, 4.2 Hz, 1H), 1.99−1.91 (m, 3H), 1.66 (d, J = 10.7 Hz, 2H), 1.52 (d, J = 8.6 Hz, 2H), 0.97 (s, 9H), 0.84−0.80 (m, 3H).^{13}C NMR (101 MHz, d_6-DMSO) δ 171.5, 169.1, 168.9, 163.0, 158.0, 151.4, 149.4, 148.8, 147.7, 142.7, 139.5, 139.3, 136.8, 132.2, 131.9, 131.1, 129.7, 128.7, 127.6, 127.4, 122.5, 121.6, 120.4, 114.8, 107.3, 69.4, 68.5, 67.6, 66.3, 64.5, 58.8, 57.8, 55.9, 55.4, 41.5, 41.2, 37.9, 35.0, 34.9, 30.3, 29.0, 26.4, 18.9, 18.2, 15.9, 14.5, 12.7. HRMS (ESI, m/z) calcd for $C_{56}H_{70}N_7O_9S$ $[M - H]^-$: 1016.4961, found: 1016.4929. Purity: 99.4%.

*N^3-((4,6-Dimethyl-2-oxo-1,2-dihydropyridin-3-yl)methyl)-$N^{4'}$-(8-(2-((2-(2,6-dioxopiperidin-3-yl)-1,3-dioxoisoindolin-4-yl)oxy)-acetamido)octyl)-5-(ethyl(tetrahydro-2H-pyran-4-yl)amino)-4-methyl-[1,1′-biphenyl]-3,4′-dicarboxamide (**G5**).* To a solution of Boc_2O (1 g, 4.58 mmol) in CH_2Cl_2 (10 mL) was added a solution of octane-1,8-diamine (2.64 g, 18.33 mmol) in CH_2Cl_2 (10 mL) dropwise at 0 °C. Then, the reaction mixture was warmed to r.t. and stirred overnight. Finally, CH_2Cl_2 (50 mL) and water (20 mL) were added. The mixture was separated, and the organic phase was washed with brine (3 × 10 mL). The organic phase was dried over Na_2SO_4 and concentrated under reduced pressure. The crude residue was purified by flash column chromatography MeOH/CH_2Cl_2 (0−10%) to give compound **37b** as a white solid (0.93 g, 63.5% yield).

To a solution of **36** (100 mg, 301 μmol) in DMF (3 mL) were added a solution of **37b** (110.3 mg, 451 μmol) in DMF (4.5 mL), DIPEA (116.69 mg, 149.22 μmol), and HATU (114.44 mg, 300.96 μmol). The reaction mixture was stirred for 19 h at r.t. and was then diluted with EtOAc (30 mL). The organic phase was washed sequentially with 10% aq. citric acid (10 mL), saturated aq. sodium bicarbonate (10 mL), water (10 mL), and brine (10 mL × 2). The organic phase was dried over Na_2SO_4, filtered, and concentrated under reduced pressure. Purification by column chromatography with MeOH/CH_2Cl_2 (0−5%) gave the desired coupling product as a yellow solid (95 mg, 56.5% yield). Then, the obtained compound was dissolved in TFA (1.5 mL, 0.1 M) and heated to 50 °C. After 1 h, the mixture was cooled to r.t., diluted with MeOH, and concentrated under reduced pressure. The crude residue was precipitated with diethyl ether and dried under vacuum to give **38b** as a yellow solid (95 mg, 100%).

To the solution of **7** (50 mg, 99.29 μmol) in DMF (2 mL) were added **38b** (71.6 mg, 119 μmol), DIPEA (73.84 μL, 446.79 μmol), and HATU (36.73 mg, 99.29 μmol). The mixture was stirred at r.t. for 22 h before EtOAc and water were added. The mixture was extracted with EtOAc twice. The combined organic phases were dried over Na_2SO_4, filtered, and concentrated under reduced pressure. The residue was purified by flash column chromatography with MeOH/CH_2Cl_2 (0−10%) to afford **G5** as a yellow solid (32 mg, 34.6% yield). ^{1}H NMR (400 MHz, d_6-DMSO) δ 11.45 (s, 1H), 11.10 (s, 1H), 8.45 (t, J = 5.5 Hz, 1H), 8.21 (t, J = 4.7 Hz, 1H), 7.91 (d, J = 8.5 Hz, 3H), 7.84−7.78 (m, 1H), 7.71 (d, J = 8.3 Hz, 2H), 7.49 (d, J = 7.2 Hz, 1H), 7.46 (s, 1H), 7.40 (d, J = 8.5 Hz, 1H), 7.29 (s, 1H), 5.86 (s, 1H), 5.12 (dd, J = 12.8, 5.4 Hz, 1H), 4.76 (s, 2H), 4.30 (d, J = 4.7 Hz, 2H), 3.83 (d, J = 10.8 Hz, 2H), 3.29−3.20 (m, 4H), 3.18−3.06 (m, 4H), 2.96−2.84 (m, 3H), 2.60−2.53 (m, 2H), 2.26 (s, 3H), 2.21 (s, 3H), 2.11 (s, 3H), 2.05 (dd, J = 12.5, 4.2 Hz, 2H), 1.67 (d, J = 11.1 Hz, 2H), 1.52 (s, 3H), 1.44 (s, 2H), 1.28 (s, 8H), 0.83 (t, J = 6.8 Hz, 3H). ^{13}C NMR (101 MHz, d_6-DMSO) δ 172.7, 169.8, 169.0, 166.7, 166.6, 165.7, 165.5, 163.0, 155.0, 149.6, 149.1, 142.8, 142.2, 139.7, 136.9, 136.3, 133.4, 133.0, 127.8, 126.3, 123.1, 121.6, 121.0, 120.4, 116.9, 116.1, 107.4, 67.7, 66.3, 57.9, 48.8, 41.2, 38.3, 34.9, 31.0, 30.3, 29.1, 29.0, 28.7, 28.7, 26.5, 26.3, 22.0, 18.9, 18.2, 14.6, 12.8. HRMS (ESI, m/z) calcd for $C_{53}H_{64}N_7O_{10}$ $[M + H]^+$: 958.4709, found: 958.4677. Purity: 96.0%.

*N^3-((4,6-Dimethyl-2-oxo-1,2-dihydropyridin-3-yl)methyl)-$N^{4'}$-(4-((2-(2,6-dioxotetrahydro-2H-pyran-3-yl)-1,3-dioxoisoindolin-4-yl)-amino)butyl)-5-(ethyl(tetrahydro-2H-pyran-4-yl)amino)-4-methyl-[1,1′-biphenyl]-3,4′-dicarboxamide (**G1**).* **G1** was prepared using the similar procedure for the synthesis of compound **G5**. ^{1}H NMR (400 MHz, d_6-DMSO) δ 11.44 (s, 1H), 11.07 (s, 1H), 8.52 (s, 1H), 8.20 (s, 1H), 7.90 (d, J = 8.4 Hz, 2H), 7.71 (d, J = 8.4 Hz, 2H), 7.60−7.53 (m, 1H), 7.46 (s, 1H), 7.29 (s, 1H), 7.12 (d, J = 8.6 Hz, 1H), 7.01 (d, J = 7.0 Hz, 1H), 6.57 (s, 1H), 5.86 (s, 1H), 5.04 (dd, J = 12.8, 5.4 Hz, 1H), 4.30 (d, J = 4.9 Hz, 2H), 3.83 (d, J = 10.4 Hz, 3H), 3.14−3.03 (m, 4H), 2.89 (dd, J = 22.5, 8.5 Hz, 2H), 2.58 (d, J = 16.9 Hz, 2H), 2.25 (s, 3H), 2.21 (d, J = 5.4 Hz, 3H), 2.11 (s, 3H), 2.08−1.99 (m, 2H), 1.65 (d, J = 20.5 Hz, 6H), 1.53 (d, J = 8.2 Hz, 2H), 0.84 (t, J = 6.9 Hz, 3H). ^{13}C NMR (101 MHz, d_6-DMSO) δ 172.8, 170.1, 169.0, 167.3, 165.8, 163.0, 149.6, 149.1, 146.4, 142.3, 139.8, 136.3, 133.4, 133.3, 132.2, 127.8, 126.4, 123.1, 121.6, 121.0, 117.3, 110.4, 109.1, 107.4, 83.9, 66.3, 57.9, 48.6, 41.6, 41.2, 34.9, 31.0, 30.3, 26.6, 26.3, 22.2, 19.0, 18.2, 14.6, 12.8. HRMS (ESI, m/z) calcd for $C_{47}H_{51}N_6O_9$ $[M - H]^-$: 843.3723, found: 843.3684. Purity: 95.2%.

*N^3-((4,6-Dimethyl-2-oxo-1,2-dihydropyridin-3-yl)methyl)-$N^{4'}$-(2-(2-((2-(2,6-dioxotetrahydro-2H-pyran-3-yl)-1,3-dioxoisoindolin-4-yl)amino)ethoxy)ethyl)-5-(ethyl(tetrahydro-2H-pyran-4-yl)amino)-4-methyl-[1,1′-biphenyl]-3,4′-dicarboxamide (**G2**).* **G2** was prepared using the similar procedure for the synthesis of compound **G5**. ^{1}H NMR (400 MHz, d_6-DMSO) δ 11.47 (s, 1H), 11.07 (s, 1H), 8.53 (t, J = 5.5 Hz, 1H), 8.21 (t, J = 4.7 Hz, 1H), 7.89 (d, J = 8.3 Hz, 2H), 7.69 (d, J = 8.4 Hz, 2H), 7.58−7.52 (m, 1H), 7.46 (s, 1H), 7.29 (s, 1H), 7.14 (d, J = 8.6 Hz, 1H), 7.01 (d, J = 7.0 Hz, 1H), 6.62 (t, J = 5.6 Hz, 1H), 5.86 (s, 1H), 5.03 (dd, J = 12.9, 5.3 Hz, 1H), 4.30 (d, J = 4.9 Hz, 2H), 3.83 (d, J = 9.6 Hz, 2H), 3.66 (t, J = 5.3 Hz, 2H), 3.61 (d, J = 6.0 Hz, 2H), 3.47 (dd, J = 10.3, 5.3 Hz, 6H), 3.10 (dd, J = 13.9, 6.8 Hz, 2H), 3.03 (s, 1H), 2.92−2.80 (m, 1H), 2.56 (d, J = 16.1 Hz, 2H), 2.25 (s, 3H), 2.21 (s, 3H), 2.11 (s, 3H), 2.04−1.94 (m, 1H), 1.67 (d, J = 10.2 Hz, 2H), 1.60−1.46 (m, 2H), 0.83 (t, J = 6.9 Hz, 3H). ^{13}C NMR (101 MHz, d_6-DMSO) δ 172.8, 170.1, 169.0, 167.3, 166.0, 163.0, 158.1, 157.8, 149.6, 149.1, 146.5, 142.8, 142.3, 139.7, 136.3, 133.5, 133.1, 132.1, 127.8, 126.4, 123.1, 121.6, 121.1, 117.5, 110.7, 109.3, 107.5, 68.8, 66.4, 57.9, 48.6, 41.7, 41.3, 34.9, 31.0, 30.4, 22.2, 19.0, 18.2, 14.7, 12.8. HRMS (ESI, m/z) calcd for $C_{47}H_{51}N_6O_{10}$ $[M - H]^-$: 859.3672, found: 859.3682. Purity: 96.7%.

*N^3-((4,6-Dimethyl-2-oxo-1,2-dihydropyridin-3-yl)methyl)-$N^{4'}$-(2-(2-(2-((2-(2,6-dioxopiperidin-3-yl)-1,3-dioxoisoindolin-4-yl)oxy)-ethoxy)ethoxy)ethyl)-5-(ethyl(tetrahydro-2H-pyran-4-yl)amino)-4-methyl-[1,1′-biphenyl]-3,4′-dicarboxamide (**G3**).* **G3** was prepared following the similar procedure for the synthesis of compound **G5**. ^{1}H NMR (400 MHz, d_6-DMSO) δ 11.46 (s, 1H), 11.09 (s, 1H), 8.52 (d, J = 5.7 Hz, 1H), 8.21 (s, 1H), 7.91 (d, J = 8.3 Hz, 2H), 7.82−7.75 (m, 1H), 7.71 (d, J = 8.2 Hz, 2H), 7.52−7.40 (m, 3H), 7.29 (s, 1H), 5.86 (s, 1H), 5.08 (dd, J = 12.8, 5.3 Hz, 1H), 4.31 (s, 4H), 3.84-3.82 (m, 3H), 3.70−3.63 (m, 2H), 3.57 (dd, J = 11.1, 5.5 Hz, 5H), 3.43 (d, J = 5.4 Hz, 2H), 3.09 (d, J = 6.8 Hz, 2H), 3.01 (d, J = 11.0 Hz, 1H), 2.94−2.79 (m, 2H), 2.63−2.53 (m, 2H), 2.26 (s, 2H), 2.21 (d, J = 5.2 Hz, 3H), 2.11 (s, 3H), 2.07 (d, J = 3.3 Hz, 1H), 2.06−1.98 (m, 2H), 1.66 (d, J = 10.2 Hz, 2H), 1.52 (d, J = 8.2 Hz, 2H), 0.83 (t, J = 6.8 Hz, 3H). ^{13}C NMR (101 MHz, d_6-DMSO) δ 172.8, 170.0, 169.0, 166.8, 165.9, 165.3, 163.0, 155.8, 149.5, 149.1, 142.8, 142.3, 139.7, 136.9, 136.2, 133.5, 133.2, 133.1, 127.8, 126.4, 123.1, 121.6, 121.0, 120.0, 116.3, 115.4, 107.4, 70.1, 69.7, 68.9, 68.9, 68.7, 66.3, 57.9, 48.8, 41.2, 34.9, 30.9, 30.3, 22.0, 18.9, 18.2, 14.6, 12.8. HRMS (ESI, m/z) calcd for $C_{49}H_{57}N_6O_{11}$ $[M + H]^+$ 905.4080, found: 905.4096. Purity: 95.0%.

*N^3-((4,6-Dimethyl-2-oxo-1,2-dihydropyridin-3-yl)methyl)-$N^{4'}$-(6-(2-((2-(2,6-dioxopiperidin-3-yl)-1,3-dioxoisoindolin-4-yl)oxy)-acetamido)hexyl)-5-(ethyl(tetrahydro-2H-pyran-4-yl)amino)-4-methyl-[1,1′-biphenyl]-3,4′-dicarboxamide (**G4**).* **G4** was prepared following the similar procedure for the synthesis of compound **G5**. ^{1}H NMR (500 MHz, d_6-DMSO) δ 11.47 (s, 1H), 11.12 (s, 1H), 8.47 (t, J = 5.3 Hz, 1H), 8.22 (t, J = 4.7 Hz, 1H), 7.95 (t, J = 5.4 Hz, 1H), 7.90 (d, J = 8.2 Hz, 2H), 7.81 (t, J = 7.9 Hz, 1H), 7.71 (d, J = 8.2 Hz, 2H), 7.51−7.43 (m, 2H), 7.39 (d, J = 8.5 Hz, 1H), 7.29 (s, 1H), 5.86 (s, 1H), 5.12 (dd, J = 12.7, 5.4 Hz, 1H), 4.77 (s, 2H), 4.30 (d, J = 4.7 Hz, 2H), 3.83 (d, J = 11.6 Hz, 2H), 3.25 (t, J = 9.3 Hz, 4H), 3.15 (dd, J = 12.5, 6.2 Hz, 2H), 3.10 (d, J = 6.9 Hz, 2H), 3.02 (t, J = 10.8 Hz, 1H), 2.90 (dd, J = 23.2, 7.3 Hz, 3H), 2.56 (dd, J = 24.7, 11.7 Hz, 2H), 2.25 (s, 3H), 2.21 (s, 3H), 2.10 (s, 3H), 2.08−2.00 (m, 1H), 1.66 (d, J = 11.1 Hz, 2H), 1.53 (d, J = 7.4 Hz, 2H), 1.45 (m, 2H), 1.31 (m, 4H), 0.83 (t, J = 6.9 Hz, 3H). ^{13}C NMR (126 MHz, d_6-DMSO) δ 172.8,

https://doi.org/10.1021/acs.jmedchem.1c00460
J. Med. Chem. 2021, 64, 10167−10184

169.9, 169.0, 166.8, 166.7, 165.8, 165.6, 163.1, 155.1, 149.6, 149.1, 142.8, 142.2, 139.8, 137.0, 136.3, 133.4, 133.1, 127.8, 126.4, 123.1, 121.6, 121.0, 120.4, 116.9, 116.1, 107.4, 67.7, 66.4, 57.9, 48.8, 41.2, 38.3, 34.9, 31.0, 30.3, 29.2, 29.0, 26.2, 26.1, 22.0, 19.0, 18.2, 14.7, 12.8. HRMS (ESI, m/z) calcd for $C_{51}H_{60}N_7O_{10}$ $[M + H]^+$: 930.4396, found: 930.4413. Purity: 95.9%.

*N^3-((4,6-Dimethyl-2-oxo-1,2-dihydropyridin-3-yl)methyl)-$N^{4'}$-(2-(2-(2-(2-((2-(2,6-dioxopiperidin-3-yl)-1,3-dioxoisoindolin-4-yl)oxy)-ethoxy)ethoxy)ethoxy)ethyl)-5-(ethyl(tetrahydro-2H-pyran-4-yl)-amino)-4-methyl-[1,1′-biphenyl]-3,4′-dicarboxamide (**G6**).* **G6** was prepared following the similar procedure for the synthesis of compound **G5**. ^{1}H NMR (400 MHz, d_6-DMSO) δ 11.45 (s, 1H), 11.09 (s, 1H), 8.52 (dd, J = 12.1, 6.3 Hz, 1H), 8.20 (t, J = 4.9 Hz, 1H), 7.90 (t, J = 9.3 Hz, 2H), 7.81−7.76 (m, 1H), 7.74−7.67 (m, 2H), 7.50 (d, J = 8.5 Hz, 1H), 7.44 (d, J = 7.3 Hz, 2H), 7.30 (s, 1H), 5.86 (s, 1H), 5.08 (dd, J = 12.8, 5.4 Hz, 1H), 4.30 (dd, J = 11.9, 6.1 Hz, 4H), 3.85 (d, J = 5.9 Hz, 1H), 3.82−3.75 (m, 2H), 3.66−3.60 (m, 2H), 3.54 (m, 8H), 3.46−3.39 (m, 2H), 3.09 (d, J = 7.0 Hz, 2H), 3.03 (s, 1H), 2.94−2.80 (m, 2H), 2.66−2.53 (m, 2H), 2.25 (s, 2H), 2.21 (d, J = 5.4 Hz, 4H), 2.10 (s, 3H), 2.09−1.97 (m, 3H), 1.90 (d, J = 11.7 Hz, 1H), 1.66 (d, J = 10.6 Hz, 1H), 1.59−1.47 (m, 2H), 0.83 (t, J = 7.0 Hz, 3H). ^{13}C NMR (101 MHz, d_6-DMSO) δ 172.7, 169.9, 166.8, 165.9, 165.2, 163.0, 155.8, 137.0, 133.2, 127.8, 126.4, 123.4, 121.5, 121.0, 120.0, 116.3, 115.4, 107.4, 99.4, 70.2, 69.8, 69.7, 69.6, 69.2, 68.9, 68.9, 68.7, 66.3, 66.1, 48.8, 34.9, 32.7, 30.9, 30.3, 22.0, 18.9, 18.9, 18.2, 14.6, 12.8. HRMS (ESI, m/z) calcd for $C_{51}H_{61}N_6O_{12}$ $[M + H]^+$: 949.4342, found 949.4323. Purity: 95.0%.

Cell Lines. The human prostate cancer cell lines 22rv1; DLBCL cell lines SU-DHL-2, SU-DHL-4, and SU-DHL-6; BL cell lines NCI-BL209, Daudi, Raji, and Namalwa; LBL cell lines JVM-2; and MCL cell lines MINO and Jeko-1 were obtained from ATCC. All cell lines were cultured in RPMI-1640, supplemented with 10% FBS at 37 °C and 5% CO_2. All of the cell lines used in the study had been tested for mycoplasma contamination every three weeks.

Cell Number Count. Cell number was counted by Cellometer Auto T4 cell counter (Nexcelom Bioscience, Lawrence, Massachusetts).

Cell Viability Assay. Cell viability was determined by the MTS assay, as we reported previously.[49]

Cell Cycle and Apoptosis. The cell cycle was measured by flow cytometry according to the commercial cell cycle analysis kit (KeyGEN BioTECH, Jiang Su, China). Annexin-V and propidium iodide-based apoptosis analyses were measured by flow cytometry according to the commercial cell apoptosis analysis kit (BD, Franklin Lakes, NJ). The activity of Caspase-3/7 was evaluated by the Caspase-Glo 3/7 Assay (Promega, Madison, WI) through the manufacturer's instructions.

Measurement of Cellular ATP. The cellular ATP concentration was detected using an ATP-based CellTiter-Glo Luminescent Cell Viability Kit (Promega, Madison, WI) according to the manufacturer's instructions.

Western Blot. The cells were washed with phosphate-buffered saline (PBS) and then lysed in lysis buffer with a protease inhibitor cocktail (Selleck). After the protein concentration normalization using a bicinchoninic acid (BCA) protein assay (ThermoFisher, Rockford, IL), the samples were separated by standard sodium dodecyl sulfate polyacrylamide gel electrophoresis (SDS-PAGE) and transferred to poly(vinylidene fluoride) (PVDF) membranes (Millipore, Billerica, MA). Subsequently, the membranes were blocked with 5% milk for 1 h at r.t. before blotting with the indicated first antibodies overnight at 4 °C. After being washed with TBST (Tris-buffered saline containing 0.1% Tween-20), the membranes were probed with the horseradish peroxidase-conjugated secondary antibodies for 1 h at r.t. Enhanced chemiluminescence was used for signal detection. The intensities of bands were performed using Image Lab (Bio-Rad, Hercules, CA). All the antibodies used for western blot are from Cell Signaling Technology.

Immunohistochemistry. Tumors were harvested in formalin and dehydrated and embedded in paraffin. Tissue slides were then deparaffinized, hydrated, and rinsed in PBS. After being boiled in citrate buffer for 4−6 min for antigen retrieval, peroxide blocking was performed with 3% H_2O_2 at r.t. for 20 min. The sections were incubated with EZH2, H3K27me3 (Cell Signaling Technology), and Ki67 (Abcam), following the suggested concentration at 37 °C overnight. Then, the samples were probed with a secondary antibody at 37 °C for 1 h. All slides were stained with 3,3′-diaminobenzidine and counterstained with hematoxylin.

Immunoprecipitation. The cells were harvested using NP40 (Beyotime Biotechnology, Shanghai, China) containing a protease inhibitor cocktail. After 30 min, cell lysates were centrifuged at 4000g for 15 min at 4 °C, and the supernatants were incubated with EZH2 antibody or IgG (Cell Signaling Technology) overnight at 4 °C. Subsequent incubation with protein A/G-coated agarose beads (Merck, Germany) continued for an additional 3 h at 4 °C. After the samples were washed six times with ice-cold NP40, the supernatants were removed by centrifugation at 800g for 2 min. The proteins were then separated from the beads using immunoblotting loading buffer for 5 min at 95 °C. The supernatants were collected for subsequent immunoblotting analysis after SDS gel separation.

Lentiviral Constructs and siRNAs. The shEZH2 lentiviral constructs were purchased from GeneCopoeia (GeneCopoeia, Inc, Rockville, Maryland) and transduced into SU-DHL-2 cells according to the literature.[15] VHL siRNA (target sequence: GCTCTACGAA-GATCTGGAA) was from RIBOBIO (Guangzhou, China). 22Rv1 cells were transfected with siRNA using Lipofectamine RNAiMAX (ThermoFisher, Rockford, IL), following the manufacturer's instructions.

Caco-2 Cell Permeability Assay. The Caco-2 cells were seeded onto polycarbonate 12-well Transwell filters at a density of 2×10^5 cells/well. The confluent monolayers obtained at 21 days were utilized to assess the in vitro permeability. Culture media in the apical and basolateral compartments were replaced every 2 days, and the integrity of the monolayer was detected by fluorescein. Before the experiments, the culture medium in both chambers was replaced with prewarmed Hank's balanced salt solution (HBSS). The cultures were then stabilized at 37 °C for 30 min. For the permeation studies, 0.2 mL of drug formulation diluted with HBSS was added to the apical side, and the basolateral side was replaced with 1 mL fresh HBSS. The treated cells were incubated at 37 ± 0.5 °C. The amount of permeated drug was determined by collecting 50 μL of samples from the basolateral compartment, followed by replacement with 50 μL of fresh HBSS at 1, 2, and 3 h. The collected samples were evaporated and reconstituted with methanol, then the concentrations of drugs in the samples were determined by liquid chromatography−mass spectrometry (LC-MS). The apparent permeability (P_{app}) of ETP in various formulations was calculated as follows: $P_{app} = \frac{dQ}{dt} \times \frac{V}{A \times C_0}$ where dQ/dt is the slope of the cumulative drug permeated versus time (μg/s), A is the surface area of the monolayer (1.12 cm^2), V is the volume of basolateral side HBSS (1 mL), and C_0 is the initial concentration of compounds on the apical side (μg/mL).

Animal Experiments. The animal experiment was conducted in compliance with a protocol approved by the Institutional Animals Care and Use Committee of Sun Yat-sen University Cancer Center and was carried out in the Center of Experiment Animal of Sun Yat-sen University (North Campus, approval no.: L102012019050K). Balb/c nude mice (female) were bought from Beijing Vital River Laboratory Animal Technology Co., Ltd. For SU-DHL-6 xenografts, and five million cells were injected subcutaneously. After 2 weeks, when tumors reached 100−200 mm^3, mice were randomly divided into three groups (6 mice per group) and administrated with a vehicle control (80% PBS, 10% castor oil, and 10% DMSO) or indicated doses of compounds (YM281: 80 mg/kg; EPZ6438: 42.5 mg/kg) through intraperitoneal injection 6 times weekly. Tumor sizes and animal weights were measured 2−3 times per week. The mice were sacrificed after 3 weeks' drug administration, and the tumor tissue was harvested for analyses. For Jeko-1 xenografts, two million cells were injected subcutaneously. Ten days later, most of the tumors grow about 100 mm^3, mice were then randomly divided into three groups

https://doi.org/10.1021/acs.jmedchem.1c00460
J. Med. Chem. 2021, 64, 10167−10184

(5 mice per group), and intraperitoneally administrated daily with the control (70% PBS, 20% castor oil, and 10% DMSO) or indicated doses of compounds (YM281: 100 mg/kg; EPZ6438: 50 mg/kg). Tumor sizes and animal weights were measured every 3 days. The mice were sacrificed after 30 days' drug treatment, and then the tumor tissue was harvested for analyses.

Isolation and Culture of Clinically Derived Lymphoma Samples. Tumor tissues from patients with lymphoma at the Sun Yat-sen University cancer center after proper informed consent were collected for cellular Caspase-3/7 activity, ATP content detection, and Western blot analyses (see Table S2 for the details of patient information). The tumor tissues were immediately minced with fine scissors, and single cells were isolated through a 70 μm strainer (BD Falcon) and cultured in RPMI-1640, supplemented with 10% FBS, 50 μM β-mercaptoethanol, and penicillin/streptomycin solution at 37 °C and 5% CO_2. Studies using human specimen were approved (No. GZR2018-089) by the Institutional Ethical Committee of Sun Yat-sen University Cancer Center.

Molecular Docking. Molecular Operating Environment (MOE 2014) (Chemical Computing Group Inc, Montreal, Quebec, Canada) was used for molecular docking. EPZ6438 was constructed using the builder module, and energy was minimized using Force Field MMFF94x and saved as the MDB file. The crystal structure of EZH2 (PDB ID: 5LS6) was downloaded from the protein data bank, and water molecules were removed. The residual crystal structure was prepared using ligX with the default parameters of MOE [gradient: 0.1, Force Field: MMFF94X]. A 5Å radius area around the bounded inhibitor in the crystal structure was defined as the active site. The prepared ligand structure was flexibly docked into the EZH2 binding site, with a triangle matcher as the placement methodology, London ΔG or ASE as a scoring methodology, force field refinement was selected, and dock calculations were run automatically. The obtained 30 conformations were generated and stored in a database, and the best conformations were analyzed for the binding interaction analysis.

Statistical Analysis. Statistical analysis was performed by GraphPad Prism 8 software (GraphPad Software, Inc, San Diego, CA). All data are presented as mean ± standard error of the mean (SEM). The statistical significance of differences was determined using Student's t-test. Differences are considered statistically significant when the p values are less than 0.05.

■ ASSOCIATED CONTENT

Supporting Information

The Supporting Information is available free of charge at https://pubs.acs.org/doi/10.1021/acs.jmedchem.1c00460.

Western blot analysis of EZH2, EZH1, and H3K27me3 levels affected by tested compounds; MTS cell viability analysis in different lymphoma cell lines treated with YM281; the structure of YM620 and its effects on EZH2 and cell proliferation; flow cytometry analysis of the cell cycle and cell apoptosis; Western blot analysis of PARP, Casp-3, and C-casp-3 levels; the body weights of the tested compound treated mice; nonsensitive cancer cell lines NIC-H460 and AsPC1 treated by the tested compounds (Figures S1−S6); patient sample information and corresponding analytical methods; apparent permeability of EPZ6438, YM181, and YM281 (Tables S1−S2); NMR spectra of V1−V7, YM620, G1−G6, and key intermediates; HRMS spectra and HPLC results of YM181 and YM281 (PDF)

The docking session for EPZ6438 in EZH2 crystal 5LS6 (PDB)

Molecular formula strings (CSV)

■ AUTHOR INFORMATION

Corresponding Authors

Peng Huang − *State Key Laboratory of Oncology in South China, Collaborative Innovation Center for Cancer Medicine, Sun Yat-sen University Cancer Center, Guangzhou 510060, China*; Phone: +86 20 87343511; Email: huangpeng@sysucc.org.cn

Shijun Wen − *State Key Laboratory of Oncology in South China, Collaborative Innovation Center for Cancer Medicine, Sun Yat-sen University Cancer Center, Guangzhou 510060, China*; orcid.org/0000-0002-9347-8243; Phone: +86 20 87342283; Email: wenshj@sysucc.org.cn

Authors

Yalin Tu − *State Key Laboratory of Oncology in South China, Collaborative Innovation Center for Cancer Medicine, Sun Yat-sen University Cancer Center, Guangzhou 510060, China*

Yameng Sun − *State Key Laboratory of Oncology in South China, Collaborative Innovation Center for Cancer Medicine, Sun Yat-sen University Cancer Center, Guangzhou 510060, China; The School of Pharmaceutical Sciences, Wuhan University, Wuhan 430071, China*

Shuang Qiao − *State Key Laboratory of Oncology in South China, Collaborative Innovation Center for Cancer Medicine, Sun Yat-sen University Cancer Center, Guangzhou 510060, China*

Yao Luo − *State Key Laboratory of Oncology in South China, Collaborative Innovation Center for Cancer Medicine, Sun Yat-sen University Cancer Center, Guangzhou 510060, China*

Panpan Liu − *State Key Laboratory of Oncology in South China, Collaborative Innovation Center for Cancer Medicine, Sun Yat-sen University Cancer Center, Guangzhou 510060, China*

Zhong-Xing Jiang − *The School of Pharmaceutical Sciences, Wuhan University, Wuhan 430071, China*; orcid.org/0000-0003-2601-4366

Yumin Hu − *State Key Laboratory of Oncology in South China, Collaborative Innovation Center for Cancer Medicine, Sun Yat-sen University Cancer Center, Guangzhou 510060, China*

Zifeng Wang − *State Key Laboratory of Oncology in South China, Collaborative Innovation Center for Cancer Medicine, Sun Yat-sen University Cancer Center, Guangzhou 510060, China*

Complete contact information is available at: https://pubs.acs.org/10.1021/acs.jmedchem.1c00460

Author Contributions

[§]Y.T., Y.S., and S.Q. contributed equally to this work.

Author Contributions

Conceptualization, S.W. and Y.T.; funding acquisition, S.W. and P.H.; methodology, Y.T., Y.S., Y.H., Z.W., and S.Q.; project administration, Y.T., Y.S., and S.Q.; resources, S.W.; Supervision, S.W. and P.H.; validation, Y.T., Y.S., and S.Q.; visualization, Y.T., Y.S., and S.Q.; writing—original draft, Y.T. and Y.S.; writing—review & editing, Y.T., S.W., P.H., and S.Q.

Notes

The authors declare no competing financial interest.

https://doi.org/10.1021/acs.jmedchem.1c00460
J. Med. Chem. 2021, 64, 10167−10184

■ ACKNOWLEDGMENTS

We are grateful for the grant support from the National Natural Science Foundation of China (81672952, 81872440), the Guangdong Science and Technology Program (2017A020215198), and the Guangzhou Science and Technology Program (201807010041).

■ ABBREVIATIONS

EZH2, enhancer of zeste homologue 2; PROTAC, proteolysis-target chimera; VHL, von Hippel−Lindau; CRBN, cereblon; DLBCL, diffuse large B-cell lymphoma; PRC2, polycomb repressive complex 2; SAM, *S*-adenosylmethionine

■ REFERENCES

(1) Margueron, R.; Reinberg, D. The Polycomb complex PRC2 and its mark in life. *Nature* **2011**, *469*, 343−349.
(2) Di Croce, L.; Helin, K. Transcriptional regulation by Polycomb group proteins. *Nat. Struct. Mol. Biol.* **2013**, *20*, 1147−1155.
(3) Velichutina, I.; Shaknovich, R.; Geng, H.; Johnson, N. A.; Gascoyne, R. D.; Melnick, A. M.; Elemento, O. EZH2-mediated epigenetic silencing in germinal center B cells contributes to proliferation and lymphomagenesis. *Blood* **2010**, *116*, 5247−5255.
(4) Ntziachristos, P.; Tsirigos, A.; Van Vlierberghe, P.; Nedjic, J.; Trimarchi, T.; Flaherty, M. S.; Ferres-Marco, D.; da Ros, V.; Tang, Z.; Siegle, J.; Asp, P.; Hadler, M.; Rigo, I.; De Keersmaecker, K.; Patel, J.; Huynh, T.; Utro, F.; Poglio, S.; Samon, J. B.; Paietta, E.; Racevskis, J.; Rowe, J. M.; Rabadan, R.; Levine, R. L.; Brown, S.; Pflumio, F.; Dominguez, M.; Ferrando, A.; Aifantis, I. Genetic inactivation of the polycomb repressive complex 2 in T cell acute lymphoblastic leukemia. *Nat. Med.* **2012**, *18*, 298−301.
(5) Xu, K.; Wu, Z. J.; Groner, A. C.; He, H. H.; Cai, C.; Lis, R. T.; Wu, X.; Stack, E. C.; Loda, M.; Liu, T.; Xu, H.; Cato, L.; Thornton, J. E.; Gregory, R. I.; Morrissey, C.; Vessella, R. L.; Montironi, R.; Magi-Galluzzi, C.; Kantoff, P. W.; Balk, S. P.; Liu, X. S.; Brown, M. EZH2 oncogenic activity in castration-resistant prostate cancer cells is Polycomb-independent. *Science* **2012**, *338*, 1465−1469.
(6) Kim, K. H.; Roberts, C. W. Targeting EZH2 in cancer. *Nat. Med.* **2016**, *22*, 128−134.
(7) Bonasio, R.; Tu, S.; Reinberg, D. Molecular signals of epigenetic states. *Science* **2010**, *330*, 612−616.
(8) Bates, S. E. Epigenetic Therapies for Cancer. *N. Engl. J. Med.* **2020**, *383*, 650−663.
(9) Kohashi, K.; Oda, Y. Oncogenic roles of SMARCB1/INI1 and its deficient tumors. *Cancer Sci.* **2017**, *108*, 547−552.
(10) Kim, K. H.; Kim, W.; Howard, T. P.; Vazquez, F.; Tsherniak, A.; Wu, J. N.; Wang, W.; Haswell, J. R.; Walensky, L. D.; Hahn, W. C.; Orkin, S. H.; Roberts, C. W. SWI/SNF-mutant cancers depend on catalytic and non-catalytic activity of EZH2. *Nat. Med.* **2015**, *21*, 1491−1496.
(11) Bitler, B. G.; Aird, K. M.; Garipov, A.; Li, H.; Amatangelo, M.; Kossenkov, A. V.; Schultz, D. C.; Liu, Q.; Shih Ie, M.; Conejo-Garcia, J. R.; Speicher, D. W.; Zhang, R. Synthetic lethality by targeting EZH2 methyltransferase activity in ARID1A-mutated cancers. *Nat. Med.* **2015**, *21*, 231−238.
(12) Yamagishi, M.; Uchimaru, K. Targeting EZH2 in cancer therapy. *Curr. Opin. Oncol.* **2017**, *29*, 375−381.
(13) First EZH2 Inhibitor Approved-for Rare Sarcoma. *Cancer Discovery* **2020**, *10*, 333 334. DOI: 10.1158/2159-8290.CD-NB2020-006.
(14) Knutson, S. K.; Wigle, T. J.; Warholic, N. M.; Sneeringer, C. J.; Allain, C. J.; Klaus, C. R.; Sacks, J. D.; Raimondi, A.; Majer, C. R.; Song, J.; Scott, M. P.; Jin, L.; Smith, J. J.; Olhava, E. J.; Chesworth, R.; Moyer, M. P.; Richon, V. M.; Copeland, R. A.; Keilhack, H.; Pollock, R. M.; Kuntz, K. W. A selective inhibitor of EZH2 blocks H3K27 methylation and kills mutant lymphoma cells. *Nat. Chem. Biol.* **2012**, *8*, 890−896.
(15) McCabe, M. T.; Ott, H. M.; Ganji, G.; Korenchuk, S.; Thompson, C.; Van Aller, G. S.; Liu, Y.; Graves, A. P.; Della Pietra, A., 3rd; Diaz, E.; LaFrance, L. V.; Mellinger, M.; Duquenne, C.; Tian, X.; Kruger, R. G.; McHugh, C. F.; Brandt, M.; Miller, W. H.; Dhanak, D.; Verma, S. K.; Tummino, P. J.; Creasy, C. L. EZH2 inhibition as a therapeutic strategy for lymphoma with EZH2-activating mutations. *Nature* **2012**, *492*, 108−112.
(16) Bate-Eya, L. T.; Gierman, H. J.; Ebus, M. E.; Koster, J.; Caron, H. N.; Versteeg, R.; Dolman, M. E. M.; Molenaar, J. J. Enhancer of zeste homologue 2 plays an important role in neuroblastoma cell survival independent of its histone methyltransferase activity. *Eur. J. Cancer* **2017**, *75*, 63−72.
(17) Kim, J.; Lee, Y.; Lu, X.; Song, B.; Fong, K. W.; Cao, Q.; Licht, J. D.; Zhao, J. C.; Yu, J. Polycomb- and Methylation-Independent Roles of EZH2 as a Transcription Activator. *Cell Rep.* **2018**, *25*, 2808−2820e4.
(18) Huang, X.; Yan, J.; Zhang, M.; Wang, Y.; Chen, Y.; Fu, X.; Wei, R.; Zheng, X. L.; Liu, Z.; Zhang, X.; Yang, H.; Hao, B.; Shen, Y. Y.; Su, Y.; Cong, X.; Huang, M.; Tan, M.; Ding, J.; Geng, M. Targeting Epigenetic Crosstalk as a Therapeutic Strategy for EZH2-Aberrant Solid Tumors. *Cell* **2018**, *175*, 186−199.e19.
(19) Gibaja, V.; Shen, F.; Harari, J.; Korn, J.; Ruddy, D.; Saenz-Vash, V.; Zhai, H.; Rejtar, T.; Paris, C. G.; Yu, Z.; Lira, M.; King, D.; Qi, W.; Keen, N.; Hassan, A. Q.; Chan, H. M. Development of secondary mutations in wild-type and mutant EZH2 alleles cooperates to confer resistance to EZH2 inhibitors. *Oncogene* **2016**, *35*, 558−566.
(20) Burslem, G. M.; Crews, C. M. Proteolysis-Targeting Chimeras as Therapeutics and Tools for Biological Discovery. *Cell* **2020**, *181*, 102−114.
(21) Lu, J.; Qian, Y.; Altieri, M.; Dong, H.; Wang, J.; Raina, K.; Hines, J.; Winkler, J. D.; Crew, A. P.; Coleman, K.; Crews, C. M. Hijacking the E3 Ubiquitin Ligase Cereblon to Efficiently Target BRD4. *Chem. Biol.* **2015**, *22*, 755−763.
(22) Winter, G. E.; Buckley, D. L.; Paulk, J.; Roberts, J. M.; Souza, A.; Dhe-Paganon, S.; Bradner, J. E. DRUG DEVELOPMENT. Phthalimide conjugation as a strategy for in vivo target protein degradation. *Science* **2015**, *348*, 1376−1381.
(23) Han, X.; Wang, C.; Qin, C.; Xiang, W.; Fernandez-Salas, E.; Yang, C. Y.; Wang, M.; Zhao, L.; Xu, T.; Chinnaswamy, K.; Delproposto, J.; Stuckey, J.; Wang, S. Discovery of ARD-69 as a Highly Potent Proteolysis Targeting Chimera (PROTAC) Degrader of Androgen Receptor (AR) for the Treatment of Prostate Cancer. *J. Med. Chem.* **2019**, *62*, 941−964.
(24) Bai, L.; Zhou, H.; Xu, R.; Zhao, Y.; Chinnaswamy, K.; McEachern, D.; Chen, J.; Yang, C. Y.; Liu, Z.; Wang, M.; Liu, L.; Jiang, H.; Wen, B.; Kumar, P.; Meagher, J. L.; Sun, D.; Stuckey, J. A.; Wang, S. A Potent and Selective Small-Molecule Degrader of STAT3 Achieves Complete Tumor Regression In Vivo. *Cancer Cell* **2019**, *36*, 498−511e17.
(25) Farnaby, W.; Koegl, M.; Roy, M. J.; Whitworth, C.; Diers, E.; Trainor, N.; Zollman, D.; Steurer, S.; Karolyi-Oezguer, J.; Riedmueller, C.; Gmaschitz, T.; Wachter, J.; Dank, C.; Galant, M.; Sharps, B.; Rumpel, K.; Traxler, E.; Gerstberger, T.; Schnitzer, R.; Petermann, O.; Greb, P.; Weinstabl, H.; Bader, G.; Zoephel, A.; Weiss-Puxbaum, A.; Ehrenhofer-Wolfer, K.; Wohrle, S.; Boehmelt, G.; Rinnenthal, J.; Arnhof, H.; Wiechens, N.; Wu, M. Y.; Owen-Hughes, T.; Ettmayer, P.; Pearson, M.; McConnell, D. B.; Ciulli, A. BAF complex vulnerabilities in cancer demonstrated via structure-based PROTAC design. *Nat. Chem. Biol.* **2019**, *15*, 672−680.
(26) Sun, Y.; Zhao, X.; Ding, N.; Gao, H.; Wu, Y.; Yang, Y.; Zhao, M.; Hwang, J.; Song, Y.; Liu, W.; Rao, Y. PROTAC-induced BTK degradation as a novel therapy for mutated BTK C481S induced ibrutinib-resistant B-cell malignancies. *Cell Res.* **2018**, *28*, 779−781.
(27) Tomaselli, D.; Mautone, N.; Mai, A.; Rotili, D. Recent advances in epigenetic proteolysis targeting chimeras (Epi-PROTACs). *Eur. J. Med. Chem.* **2020**, *207*, No. 112750.
(28) Vogelmann, A.; Robaa, D.; Sippl, W.; Jung, M. Proteolysis targeting chimeras (PROTACs) for epigenetics research. *Curr. Opin. Chem. Biol.* **2020**, *57*, 8−16.

(29) Wen, S.; Wang, J.; Liu, P.; Li, Y.; Lu, W.; Hu, Y.; Liu, J.; He, Z.; Huang, P. Novel combination of histone methylation modulators with therapeutic synergy against acute myeloid leukemia in vitro and in vivo. *Cancer Lett.* **2018**, *413*, 35−45.
(30) Kuntz, K. W.; Campbell, J. E.; Keilhack, H.; Pollock, R. M.; Knutson, S. K.; Porter-Scott, M.; Richon, V. M.; Sneeringer, C. J.; Wigle, T. J.; Allain, C. J.; Majer, C. R.; Moyer, M. P.; Copeland, R. A.; Chesworth, R. The Importance of Being Me: Magic Methyls, Methyltransferase Inhibitors, and the Discovery of Tazemetostat. *J. Med. Chem.* **2016**, *59*, 1556−1564.
(31) Galdeano, C.; Gadd, M. S.; Soares, P.; Scaffidi, S.; Van Molle, I.; Birced, I.; Hewitt, S.; Dias, D. M.; Ciulli, A. Structure-guided design and optimization of small molecules targeting the protein-protein interaction between the von Hippel-Lindau (VHL) E3 ubiquitin ligase and the hypoxia inducible factor (HIF) alpha subunit with in vitro nanomolar affinities. *J. Med. Chem.* **2014**, *57*, 8657−8663.
(32) Frost, J.; Galdeano, C.; Soares, P.; Gadd, M. S.; Grzes, K. M.; Ellis, L.; Epemolu, O.; Shimamura, S.; Bantscheff, M.; Grandi, P.; Read, K. D.; Cantrell, D. A.; Rocha, S.; Ciulli, A. Potent and selective chemical probe of hypoxic signalling downstream of HIF-alpha hydroxylation via VHL inhibition. *Nat. Commun.* **2016**, *7*, No. 13312.
(33) Zorba, A.; Nguyen, C.; Xu, Y.; Starr, J.; Borzilleri, K.; Smith, J.; Zhu, H.; Farley, K. A.; Ding, W.; Schiemer, J.; Feng, X.; Chang, J. S.; Uccello, D. P.; Young, J. A.; Garcia-Irrizary, C. N.; Czabaniuk, L.; Schuff, B.; Oliver, R.; Montgomery, J.; Hayward, M. M.; Coe, J.; Chen, J.; Niosi, M.; Luthra, S.; Shah, J. C.; El-Kattan, A.; Qiu, X.; West, G. M.; Noe, M. C.; Shanmugasundaram, V.; Gilbert, A. M.; Brown, M. F.; Calabrese, M. F. Delineating the role of cooperativity in the design of potent PROTACs for BTK. *Proc. Natl. Acad. Sci. U.S.A.* **2018**, *115*, E7285−E7292.
(34) Bondeson, D. P.; Smith, B. E.; Burslem, G. M.; Buhimschi, A. D.; Hines, J.; Jaime-Figueroa, S.; Wang, J.; Hamman, B. D.; Ishchenko, A.; Crews, C. M. Lessons in PROTAC Design from Selective Degradation with a Promiscuous Warhead. *Cell Chem. Biol.* **2018**, *25*, 78−87.e5.
(35) Schapira, M.; Calabrese, M. F.; Bullock, A. N.; Crews, C. M. Targeted protein degradation: expanding the toolbox. *Nat. Rev. Drug Discovery* **2019**, *18*, 949−963.
(36) Zoppi, V.; Hughes, S. J.; Maniaci, C.; Testa, A.; Gmaschitz, T.; Wieshofer, C.; Koegl, M.; Riching, K. M.; Daniels, D. L.; Spallarossa, A.; Ciulli, A. Iterative Design and Optimization of Initially Inactive Proteolysis Targeting Chimeras (PROTACs) Identify VZ185 as a Potent, Fast, and Selective von Hippel-Lindau (VHL) Based Dual Degrader Probe of BRD9 and BRD7. *J. Med. Chem.* **2019**, *62*, 699−726.
(37) Potjewyd, F.; Turner, A. W.; Beri, J.; Rectenwald, J. M.; Norris-Drouin, J. L.; Cholensky, S. H.; Margolis, D. M.; Pearce, K. H.; Herring, L. E.; James, L. I. Degradation of Polycomb Repressive Complex 2 with an EED-Targeted Bivalent Chemical Degrader. *Cell Chem. Biol.* **2020**, *27*, 47−56.e15.
(38) Hsu, J. H.; Rasmusson, T.; Robinson, J.; Pachl, F.; Read, J.; Kawatkar, S.; DH, O. D.; Bagal, S.; Code, E.; Rawlins, P.; Argyrou, A.; Tomlinson, R.; Gao, N.; Zhu, X.; Chiarparin, E.; Jacques, K.; Shen, M.; Woods, H.; Bednarski, E.; Wilson, D. M.; Drew, L.; Castaldi, M. P.; Fawell, S.; Bloecher, A. EED-Targeted PROTACs Degrade EED, EZH2, and SUZ12 in the PRC2 Complex. *Cell Chem. Biol.* **2020**, *27*, 41−46.e17.
(39) Maniaci, C.; Hughes, S. J.; Testa, A.; Chen, W.; Lamont, D. J.; Rocha, S.; Alessi, D. R.; Romeo, R.; Ciulli, A. Homo-PROTACs: bivalent small-molecule dimerizers of the VHL E3 ubiquitin ligase to induce self-degradation. *Nat. Commun.* **2017**, *8*, No. 830.
(40) Knutson, S. K.; Warholic, N. M.; Wigle, T. J.; Klaus, C. R.; Allain, C. J.; Raimondi, A.; Porter Scott, M.; Chesworth, R.; Moyer, M. P.; Copeland, R. A.; Richon, V. M.; Pollock, R. M.; Kuntz, K. W.; Keilhack, H. Durable tumor regression in genetically altered malignant rhabdoid tumors by inhibition of methyltransferase EZH2. *Proc. Natl. Acad. Sci. U.S.A.* **2013**, *110*, 7922−7927.
(41) Remillard, D.; Buckley, D. L.; Paulk, J.; Brien, G. L.; Sonnett, M.; Seo, H. S.; Dastjerdi, S.; Wuhr, M.; Dhe-Paganon, S.; Armstrong, S. A.; Bradner, J. E. Degradation of the BAF Complex Factor BRD9 by Heterobifunctional Ligands. *Angew. Chem., Int. Ed.* **2017**, *56*, 5738−5743.
(42) Zhou, B.; Hu, J.; Xu, F.; Chen, Z.; Bai, L.; Fernandez-Salas, E.; Lin, M.; Liu, L.; Yang, C. Y.; Zhao, Y.; McEachern, D.; Przybranowski, S.; Wen, B.; Sun, D.; Wang, S. Discovery of a Small-Molecule Degrader of Bromodomain and Extra-Terminal (BET) Proteins with Picomolar Cellular Potencies and Capable of Achieving Tumor Regression. *J. Med. Chem.* **2018**, *61*, 462−481.
(43) Zengerle, M.; Chan, K. H.; Ciulli, A. Selective Small Molecule Induced Degradation of the BET Bromodomain Protein BRD4. *ACS Chem. Biol.* **2015**, *10*, 1770−1777.
(44) Wang, X.; Cao, W.; Zhang, J.; Yan, M.; Xu, Q.; Wu, X.; Wan, L.; Zhang, Z.; Zhang, C.; Qin, X.; Xiao, M.; Ye, D.; Liu, Y.; Han, Z.; Wang, S.; Mao, L.; Wei, W.; Chen, W. A covalently bound inhibitor triggers EZH2 degradation through CHIP-mediated ubiquitination. *EMBO J.* **2017**, *36*, 1243−1260.
(45) Kasibhatla, S.; Jessen, K. A.; Maliartchouk, S.; Wang, J. Y.; English, N. M.; Drewe, J.; Qiu, L.; Archer, S. P.; Ponce, A. E.; Sirisoma, N.; Jiang, S.; Zhang, H. Z.; Gehlsen, K. R.; Cai, S. X.; Green, D. R.; Tseng, B. A role for transferrin receptor in triggering apoptosis when targeted with gambogic acid. *Proc. Natl. Acad. Sci. U.S.A.* **2005**, *102*, 12095−12100.
(46) Ma, A.; Stratikopoulos, E.; Park, K. S.; Wei, J.; Martin, T. C.; Yang, X.; Schwarz, M.; Leshchenko, V.; Rialdi, A.; Dale, B.; Lagana, A.; Guccione, E.; Parekh, S.; Parsons, R.; Jin, J. Discovery of a first-in-class EZH2 selective degrader. *Nat. Chem. Biol.* **2020**, *16*, 214−222.
(47) Huang, H. T.; Dobrovolsky, D.; Paulk, J.; Yang, G.; Weisberg, E. L.; Doctor, Z. M.; Buckley, D. L.; Cho, J. H.; Ko, E.; Jang, J.; Shi, K.; Choi, H. G.; Griffin, J. D.; Li, Y.; Treon, S. P.; Fischer, E. S.; Bradner, J. E.; Tan, L.; Gray, N. S. A Chemoproteomic Approach to Query the Degradable Kinome Using a Multi-kinase Degrader. *Cell Chem. Biol.* **2018**, *25*, 88−99.e6.
(48) Liu, Z.; Hu, X.; Wang, Q.; Wu, X.; Zhang, Q.; Wei, W.; Su, X.; He, H.; Zhou, S.; Hu, R.; Ye, T.; Zhu, Y.; Wang, N.; Yu, L. Design and Synthesis of EZH2-Based PROTACs to Degrade the PRC2 Complex for Targeting the Noncatalytic Activity of EZH2. *J. Med. Chem.* **2021**, *64*, 2829−2848.
(49) Yang, M.; Liu, P.; Wang, K.; Glorieux, C.; Hu, Y.; Wen, S.; Jiang, W.; Huang, P. Chemotherapy induces tumor immune evasion by upregulation of programmed cell death ligand 1 expression in bone marrow stromal cells. *Mol. Oncol.* **2017**, *11*, 358−372.

https://doi.org/10.1021/acs.jmedchem.1c00460
J. Med. Chem. 2021, 64, 10167−10184